T.C.

AYDIN ADNAN MENDERES UNIVERSITY

GRADUATE SCHOOL OF NATURAL AND APPLIED SCIENCES

MASTER'S PROGRAMME IN MECHANICAL ENGINEERING

THERMAL DESIGN AND OPTIMIZATION OF SHELL AND TUBE HEAT EXCHANGER THROUGH METAHEURISTIC ALGORITHMS

HAYRULLAH BİLGERAN YEŞİLÖZ

MASTER'S THESIS

SUPERVISOR

Assoc. Prof. Dr. Mustafa ASKER

Assoc. Prof. Dr. Oğuz Emrah TURGUT

AYDIN-2022

ACKNOWLEDGEMENTS

I would like to express my gratitude to my sincere supervisors, Assoc. Prof. Dr. Mustafa ASKER and Assoc. Prof. Dr. Oğuz Emrah TURGUT who were offered invaluable support with their sincerity and belief in me. I am also grateful to my friend Berke Emrecan ARSLAN for his advice and comments about algorithm.

I would like to give all my special thanks to my beloved mother and father for their supports.

Hayrullah Bilgeran YEŞİLÖZ

TABLE OF CONTENTS

LIST OF SYMBOLS AND ABBREVATIONS

A_1 : Current location of the best first vulture

ρ_{np} : Density of nanoparticles

$d(t)$: Distance between a vultures

C_E : Energy cost

f : Fanning friction factor

$A_{o,w}$: Flow area in the window section

f_{id} : Friction factor related to crossflow fluid

σ : Function of the contraction ratio

ε : Heat exchanger effectiveness

X_l : Longitudinal tube pitch

N_b : Number of baffles

$iter$: Number of iterations

N_{pass} : Number of passes

N_{ss} : Number of sealing strip pairs

n_p : Number of tube passes

N : Number of vultures

d_o : Outer tube diameter

U_o : Overall heat transfer coefficient

PP : Overall pumping power

Δp_{cr} : Pressure drop in the central (crossflow) section

Δp_{i-o} : Pressure drop in the shell-side inlet and outlet sections

Δp_w : Pressure drop in the window area

F : Rate of vultures being satiated

D_s : Shell side diameter

h_s : Shell side heat transfer coefficient

$(C_p)_{nf}$: Specific heat of the nanofluids

K_c : Sudden contraction coefficients

K_e : Sudden expansion coefficients

N_t : The number of tubes

k_w : The thermal conductivity of the tube wall

C_{tot} : Total cost of heat exchanger

C_{oD} : Total discounted operating cost

Q : Total heat transfer rate

Δp_s : Total shell side pressure drops

L_t : Total tube length

Δp_t : Total tube side pressure drops

X_t : Transverse tube pitch

p_t : Tube pitch

$T_{t,i}$: Tube side inlet temperatures

Pr_t : Tube side Prandtl number

$A_{o,t}$: Tube side total heat transfer area

δ_{tb} : Tube-to-baffle clearance

μ_{bf} : Viscosity of base fluids

μ_{nf} : Viscosity of nanofluid

φ_v : Volume concentration of the solid particles (nanoparticle ratio)

δ_{sb} : Shell-to-baffle clearance

H : Annual amount of operating hours

C_o : Annual operating cost

C_i : Capital investment cost

j_i : Colburn j-factor for an ideal tube bank and the correlation

J_r : Correction factor for any adverse temperature gradient buildup in laminar flows

J_c : Correction factor for baffle configuration

J_l : Correction factor for baffle leakage effects

J_b : Correction factor for bundle and pass partition bypass streams

J_s : Correction factor for larger baffle spacing at the inlet and outlet sections

A_2 : Current location of the second-best vulture

ρ_{bf} : Density of base fluid

ρ_{nf} : Density of nanofluids

d_i : Inner tube diameter

$Levy(d)$: Levy flight motion

C : Minimum value between shell and tube side heat capacities

Nu_{nf} : Nusselt number of nanofluids

$\Delta p_{w,id}$: Pressure drop concerned with one window section

$\Delta p_{b,id}$: Pressure drop that occurred in a crossflow between two baffles

$rand$: Random number

$T_{s,i}$: Shell side inlet temperatures

G_s : Shell side mass velocity

$\mathbf{Re}_s$: Shell side Reynold number

k_{bf} : Thermal conductivity of base fluid

k_{np} : Thermal conductivity of nano particles

k_{nf} : Thermal conductivity of nanofluids

$thck$: Thickness of tubes

A_o : Total heat transfer area

T_{layout} : Tube layout

h_t : Tube side heat transfer coefficient

$\mathbf{Re}_t$: Tube side Reynold number

S_1, S_2 : Rotary flight strategy

$A_{o,bp}$: Magnitude of crossflow area for flow bypass

$A_{o,tb}$: Total tube-to-baffle leakage area

F_c : Total number of tubes in the crossflow section.

$L_{b,c}$: Baffle spacing at the center.

$L_{b,i}$: Baffle spacing at the inlet,

$L_{b,o}$: Baffle spacing at the outlet

$N_{r,cw}$:Number of tube rows in crossflow

$A_{o,cr}$: Crossflow area

$A_{o,sb}$: Shell-to-baffle leakage area

$N_{r,cc}$: Effective tube rows in crossflow

AVOA : African Vultures Optimization Algorithm

$f(x)$: Objective function

HVAC : Heating, Ventilating and Air Conditioning

LF : Levy Flight

PSO : Particle Swarm Optimization

STHE : Shell and Tube Heat Exchanger

TEMA : The Tubular Exchanger Manufacturers Association

WOA : Whale Optimization Algorithm

w_p **:** Width of bypass lane

LIST OF FIGURES

LIST OF TABLES

ÖZET

METASEZGİSEL ALGORITMALAR KULLANARAK GÖVDE BORU TİPLİ BIR ISI DEĞİŞTRİCİNİN ISIL TASARIMI VE OPTİMİZASYONU

Hayrullah Bilgeran Y. Aydın Adnan Menderes Üniversitesi, Fen Bilimleri Enstitüsü, Makine Mühendisliği Programı, Yüksek Lisans Tezi, Aydın, 2022

Amaç: Bu araştırma Afrika Akbaba Optimizasyon Algoritması (AVOA) olarak adlandırılan Metasezgisel Algoritmaları uygulayarak altı farklı nano-akışkan ile ısıl performansı ve bir gövde-boru tipi ısı değiştiricinin optimizasyonunu araştırmak amacı ile yapılmıştır.

Materyal ve Yöntem: Her altı nano-parçacıklı ısı değiştirici simülasyonu için otuz adet birbirinden bağımsız simülasyon sonucu AVOA aracılığı ile elde edilmiştir. Elde edilen sayısal verilere istatikstik analiz testi uygulanmış ve sonuçların kesinliği araştırılmıştır. Ardından her farklı nano-akışkan kullanılan ısı değiştirici simülasyonu için elde edilen sayısal sonuçlar karşılaştırılmıştır. Son aşama olarak, çalışma durumunda en düşük toplam maliyeti elde edilen nano-parçacığı kullanılan sistem için bir duyarlılık testi yapılmıştır.

Bulgular: SiO_2 bazlı nanoakışkan, diğer seçenekler arasında en yüksek ısı transfer katsayısını vermiştir, SiO_2 nanoparçacıkları ile yapılan çalışma, AVOA'da en kararlı sonuçları vermiştir ve 1321,44 ile en düşük standart sapma sonucunu almıştır. Su – SiO_2 nanoakışkanı aynı zamanda 21116,83 € ile en düşük maliyeti vermiştir.

Sonuç: SiO_2'nin algoritmadaki en kararlı nanoparçacık olduğu kanıtlanmış olmakla birlikte, SiO2 diğer seçeneklerin yanı sıra gerçek dünyadaki bir mühendislik problemi için en uygun çözümü sağmıştır. SiO_2, bir kabuk-boru ısı eşanjörü için diğer nanoparçacıklara göre üstünlüğünü kanıtlıyor.

Anahtar kelimeler: Gövde-borulu ısı değiştirici, İstatistiksel analiz, Metasezgisel algoritmalar, Nano-akışkanlar, Sayısal simülasyon, Termal tasarım.

ABSTRACT

THERMAL DESIGN AND OPTIMIZATION OF SHELL AND TUBE HEAT EXCHANGER THROUGH METAHEURISTIC ALGORITHMS

Hayrullah Bilgeran Y. Aydın Adnan Menderes University, Graduate School of Natural and Applied Sciences, Mechanical Engineering Program, Master Thesis, Aydın, 2022

Objective: The purpose of this thesis is to investigate the thermal performance of a shell and tube heat exchanger with six various nanofluids and optimization by applying Metaheuristic Algorithms called African Vulture Optimization Algorithm (AVOA).

Material and Methods: Since metaheuristic methods are algorithms with stochastic characteristics, thirty independent simulation results for each six nanoparticle heat exchanger simulation were obtained by AVOA. In order to measure the stability of independent results, statistical analysis test was applied to the obtained numerical data and the precision of the results was investigated. Then, the numerical results obtained for the heat exchanger simulation using each different nanofluid was compared. As the last phase, a sensitivity test was performed.

Results: SiO_2 based nanofluid was obtained the highest heat transfer coefficient among other options, the study with SiO_2 nanoparticles were obtained the most stable results in AVOA, and were gotten the lowest standard deviation result of 1321.44. Water – SiO_2 nanofluid was obtained the lowest cost with 21116.83 €.

Conclusion: Along with, SiO_2 has proven to be the most stable nanoparticle in the algorithm, SiO_2, among other options, provides the optimal solution for a real-world engineering problem. SiO_2 proving its superiority over other nanoparticles for a shell-and-tube heat exchanger.

Keywords: Metaheuristic algorithms, Nanofluids, Numerical simulation, Shell and tube heat exchanger, Statistical analysis, Thermal design.

1. INTRODUCTION

Energy is utilized in line with the advantages of human being in history by turning into to one from another. Additionally, ways of usage efficiently and effectively are sought. Energy can be defined as the capacity for doing work and it can be divided into different types. Heat (Thermal) energy, chemical energy, nuclear energy, electrical energy can be given as examples of these types. Today, new methods of production and storage are developing rapidly with the spread and development of technology, for the types of applicable and storable. In addition, it is transformed into a better, more advantageous and more efficient by improving current methods. The usage variations of energy and modes of transport increase in a decade, due to spreading of humanity to almost every part of the world. This situation causes the consumption of energy increasingly. However, waste of energy is much more than the energy that is consumed by us. In addition, most of the processes to produce internal energy, leave behind unusable waste essential energy. For this reason, projects and researches about the conservation or revaluation of lost energy are of great importance for many engineers, analyst, and scientists (Ram *et al.*, 2022).

Losses take place in various essential energy types as chemical energy, electrical energy or heat (thermal) energy. As these losses for electric energy and chemical energy generally occur by turning into heat energy, and then, heat energy losses occur when the environment desired to be used interacts with the surroundings and transfers the existing energy to the external environment by means of the laws of thermodynamics. Although, there are various implementation for conservation or revaluation of lost energy of other essential energy types, in addition to being an appliance frequently used in daily life heat exchangers which get tackled in this article, are one of most significant appliances for heat energy to prevent, oriented and re-evaluate.

Heat exchangers are appliances utilized in umpteen areas in our life and have many different types and shapes. The wide usage area of heat exchangers attracted many engineers to research and develop heat exchangers. Academic definition of heat exchangers can be expressed as sophisticated devices that are used to transfer thermal energy. Basically, these devices are able to transfer heat between two or more fluids, between a solid surface and a fluid, or between solid particulates and fluid at different temperatures and in thermal

contacts (Dubey *et al.*, 2014). It is probable to see these devices in daily lives. Air conditioners, radiators, refrigerators can be given as examples of these devices. However, heat exchangers are used mostly in industrial applications such as steam generators in thermal power plants, distillers in the chemical industry, evaporators and condensers in HVAC applications and refrigeration process, electronic heat sinks, automobile radiators, regenerators in gas turbine engines. Every kind of heat exchanger needs calculation, optimization and development processes according to their usage areas (Tubular Heat Exchangers Manufacturers Association, 1999). It should be taken into account that optimizations and development of heat exchangers is a significant pas for usage most effectively and efficiently, reduction of energy losses and re-evaluation in order to prevent as much energy as possible for the intended use. Calculation, optimization and development processes that mentioned are created with some specific phases and research. First, thermal design analysis of a heat exchanger is conducted (ETSU, 2000). Then heat exchanger is created according to data of first step with design optimization and utilizing different refrigerants to improve the heat exchanger efficiency. Also, the total cost can be determined end evaluate approximately. At the end of the research, the results are evaluated as considering data obtained. In some of phases, the amount of data and variables that must be evaluated are as much and complicated as not to be calculated by normal and known mathematical operations. This complexity and variables that must be evaluated are, specified in Sections 3.3 and 3.4. Calculation of complex and arduous problems can be solved by using a set of algorithms called “metaheuristic algorithms” that be able to assist to complex calculations.

1.1. Metaheuristic Algorithms

Technological devices and machines have become more comprehensive and useful in decades. Developing and producing of these technological devices and machines, transform complex and arduous. In spite of that, the evolution of resolving complex problems is also indicate improvement. As a one of the best resolutions to solve problems, metaheuristic algorithms, are significant area that has grown dramatically to solve these various problems, continuous and intangible optimizations.

Metaheuristic algorithms are a decision mechanism that works on algorithms which are basically not precise in their work, do not always work with the same performance or always guarantee results, but are still useful algorithms for optimizing the problem. Metaheuristics sample a set of solutions which is otherwise overlarge to be completely enumerated or otherwise explored. Metaheuristics might build comparatively few assumptions concerning the optimization drawback being solved so could also be usable for a spread of issues (Blum and Roli, 2003). Today, more than one method has been developed for any kind of solutions in many areas and these methods have been improved according to the problem. However, the need to choose between more than one solutions method for a problem is eliminated in this way. Simply a metaheuristic algorithm selects between these algorithms and runs the most successful.

Metaheuristic algorithms cannot be said to be purely human-based algorithms. Some metaheuristic algorithms have been created with inspiration from nature as like human beings design machines inspired by nature during history. By observing searching best place, eating and hunting of animal's behavior, solving problems skills are transformed into statistic data. After this process, mathematic and optimization problems are solved by formalizing these data. Particle Swarm Optimization (PSO) is one of the algorithms which can be given as an example to inspire from nature. If it needs to be mentioned briefly, it is developed from swarm intelligence and is inspired by the research of bird and fish flock movement behavior. While searching or hunting for food, the birds are either dispersed or move together before they locate the place where they are able to find the food (Gopal *et al.*, 2020). Based on this behavior, in the algorithm, it is created a swarm consisting of particles that has random position and they search possible global best iteration by iteration. In addition, every particle informs the others and compares data with other particles data, as like birds and fish flock. Therefore, they reach the global best. One other instance of algorithms inspired by nature is Whale Optimization Algorithm (WOA). This algorithm, as the name suggests, is inspired by a whale's hunting behavior. These creatures force a flock of prey to become spheres shape by using a formed bubble wall which is created by the whale itself, and by revolving around its prey. Then they attack their prey by shrinking bubble walls in a spiral shape. Based on the whale's behavior, firstly, it is generated three-dimensional space for the study case that wanted to examine. In three-dimensional space, a random position is assumed the best position. Also, this position represents a whale. After that, the global best is determined by applying the circle reduction method or spiral

shrinking method. (Gharehchopogh and Gholizadeh, 2019) Another instance of animal-based metaheuristic algorithm is African Vultures Optimization Algorithm (AVOA) which forms the cornerstone of this thesis. Unlike other metaheuristic algorithms, details and mathematical modelling will be detailed in Section 3.4.

1.2. Heat Exchangers Types and Their Usage Areas

A heat exchanger is a system used to transfer heat between two or more fluids. Heat exchangers are used in both cooling and heating processes. The fluids may be separated by a solid wall to prevent mixing or they may be in direct contact. Generally, heat exchangers are classified in four subheads by structural features

1.2.1. Plate Type Heat Exchangers

Plate-type heat exchangers are formed by the assembly of thin plates. The plates can be flat or have some form of canals. These exchangers are not appropriate systems having very high pressures, temperatures or pressure and temperature differences. Plate heat exchangers can be divided into three different types, including gasketed plate, spiral plate and lamella. Gasketed plate heat exchangers consist of merged thin metal plates. It includes holes on the plate at four corners for fluid to cross. Fluids are orientated by pressure to mix using suitable gaskets as shown in Figure 1.1. Package is compressed by compression bolts. Capacity can be changed by adding or subtracting plate (Smith, 2005).

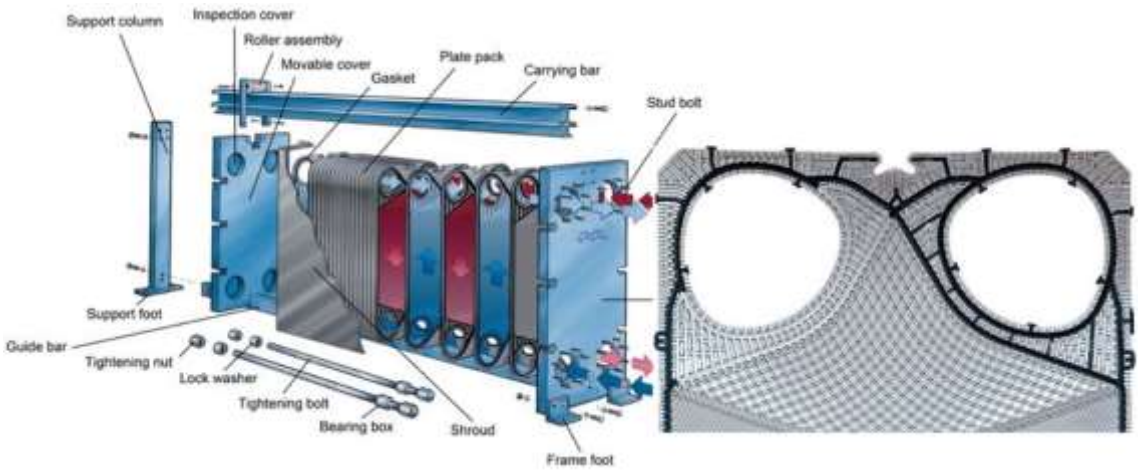

Figure 1.1. Gasketed plate heat exchanger (Bright Hub Engineering, 2010).

Spiral plate heat exchangers are a sort of heat exchangers that are generated with two relatively long strips of sheet metal wrapped helically to form a pair of spiral channels for two fluids and as illustrated in Figure 1.2. The spiral turns cause heat exchangers to have relatively large diameter. The heat transfer coefficients are not as high as plate types but higher than that for a STHE (Shah and Sekuli, 2003).

Lamella heat exchangers includes an outer tubular shell surrounding an inside bundle of elements which are flat tubes (Fig. 3). These exchangers are preferred generally for pulp and paper industry.

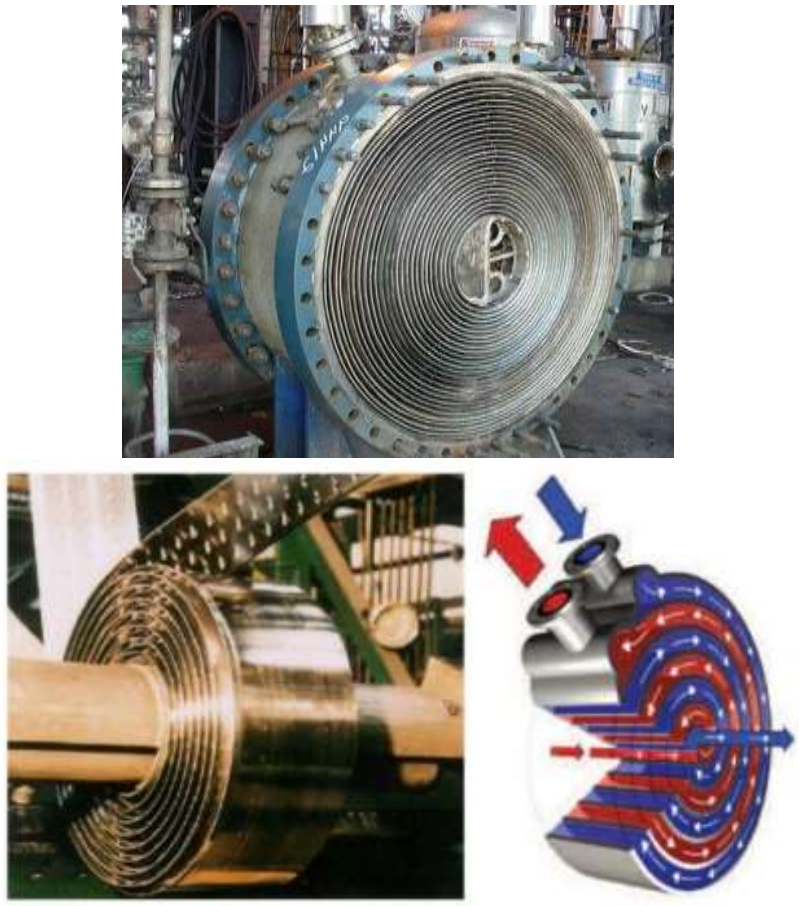

Figure 1.2. Spiral plate heat exchanger. (Fan et al., 2013; Spiral Heat Exchanger Internal, 2018;).

Figure 1.3. Lamella heat exchanger. (Lamella Heat Exchangers, 1999).

1.2.2. Extended Surface Heat Exchangers

This sort of heat exchanger models is preferred for the state that high heat exchanger efficiency. In addition, they are more compact heat exchangers are needed. Extended surface exchangers can be tackled into plate-fin and tube-fin exchangers. Plates are grooved to increase surface area for plate finned type. Ventilation radiators cane be given as an instance for this case. For the tube-finned Tubes includes annular fins to expand the surface area as seen in Figure 1.4.

Figure 1.4. Extended surface heat exchanger. (Shah and Sekulic, 2003).

1.2.3. Regenerators

Regenerators are known as storage type heat exchangers. These types of heat exchangers can be categorized into rotary type (Fig. 1.5), fixed matrix, periodic flow regenerators and heat accumulators. The main vantage of the regenerator is being more compact and economical with respect to recuperators. The reason is the separation of hot and cold gas streams via radial gaskets or valves.

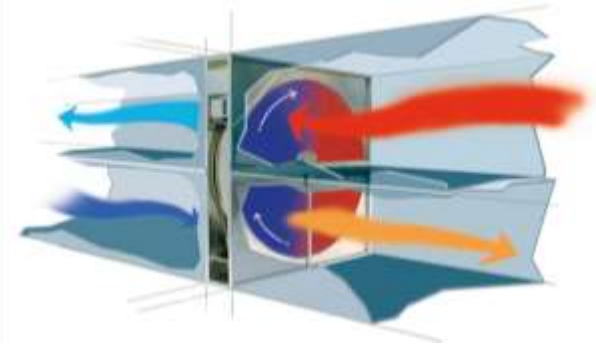

Figure 1.5. Rotary type regenerator (Rotary Type Regenerator, 2016).

1.2.4. Shell and Tube Heat Exchangers (STHE)

These are the most commonly used type of exchanger in refineries and petrochemical plants. They are cost effective for moderate to large applications, are relatively easy to clean, can be custom designed and different types of design and configuration are available including cross-flow and true counter-current flow.

STHE are generally composition of a bundle of round tubes mounted in a cylindrical shell. The major components are tubes, shell, front end head, rear end head, baffles and tube sheets (Fig. 1.6). Tubular heat exchangers are generally preferred in industry because of being compatible to generate for any capacity and operation conditions.

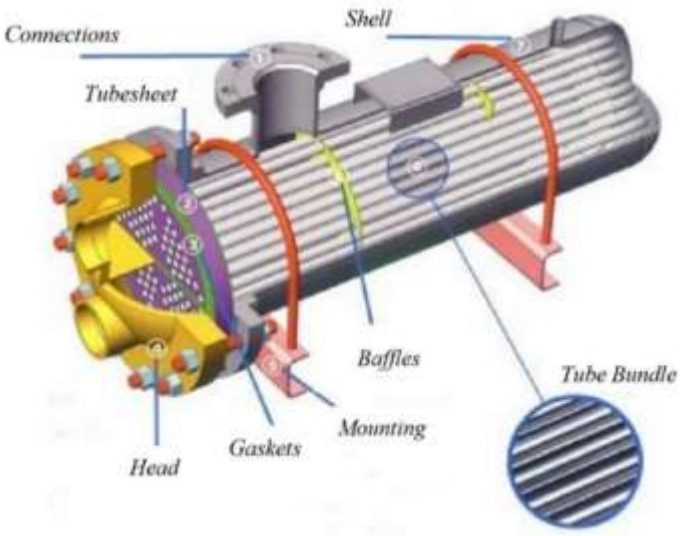

Figure 1.6. Shell and Tube Heat Exchanger. (Heat Exchanger, Space heating equipment, 2015).

Standard shell, front and rear end head types can be seen in Figure 1.7. These type standards are created by a trade association called The Tubular Exchanger Manufacturers Association (TEMA). TEMA also have pioneered the research and development of heat exchangers for over sixty years.

As it seen in Figure 1.7, TEMA designations refer to portions of the unit that make up the complete heat exchanger. If it needs to be given an example, for the TEMA Type NFU; the “N” represents the front head, the “F” the core or middle section, and “U” represents the rear head designs.

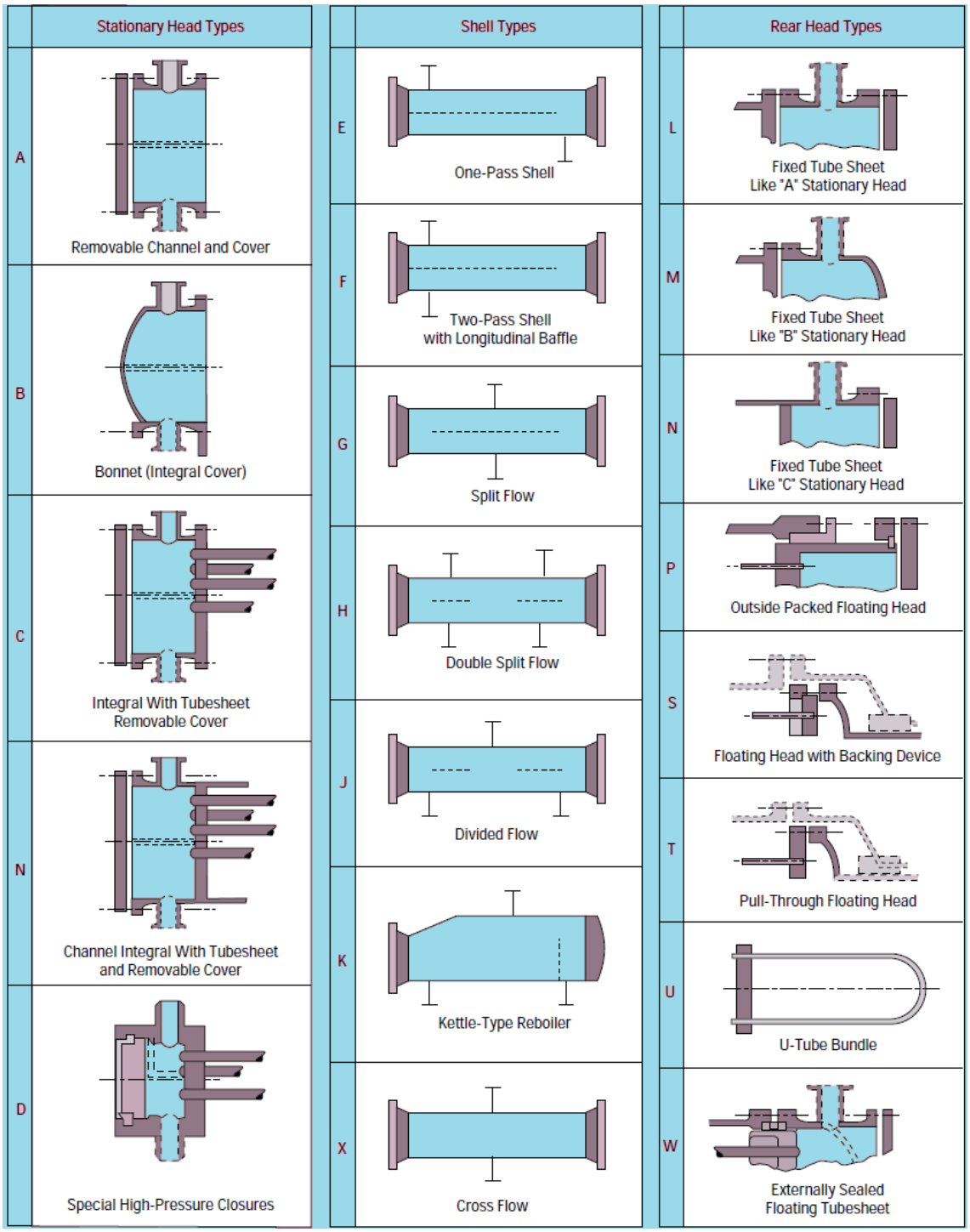

Figure 1.7. The Diagram of STHE Defined by TEMA. (Shell & tube heat exchanger - EnggCyclopedia, 2011).

2. LITERATURE REVIEW

Many researchers have been investigated the analysis of shell and tube heat exchanger devoted themselves in order to improve its performance. In addition, there are review and comparison studies on heat exchangers by caried out by engineers and academic. The examination topic based on optimization of shell and tube heat exchanger also using the metaheuristic algorithms in optimization attract attention many researchers. Some research relative to topic of this paper is mentioned below;

Kayabasi et al. (2019) investigated the effects of geometric properties such as baffle spacing, baffle cut, sealing strips, gaps between heat exchanger components, number of tubes and tube passes for shell and tube heat exchangers, by obtaining geometrical dimensions and data of a specific heat exchanger used in an industrial application. Also, they analyzed the reference heat exchanger by utilizing a software called HTRI Xchanger Suite Educational. Their results indicated that tube side pressure losses raise rapidly with the increase of the number of tube side passes. Because of the number of tubes determines the shell diameter, it is caused that using the minimum baffle spacing especially in heat exchangers with few tubes results in higher pressure losses. In addition, they determined the highest heat transfer coefficient versus unit pressure losses by using 0.6 times of shell inner diameter as baffle spacing and 25% baffle cut according to software analysis.

Fesanghary et al. (2009) examined the use of global sensitivity analysis (GSA) and harmony search algorithm (HSA) for design optimization of shell and tube heat exchangers (STHXs) from the economic viewpoint. They defined that non-influential geometrical parameter which have the least effect on total cost of STHXs, by using GSA. After that, they applied the HSA which is a meta-heuristic-based algorithm to optimize the influential geometrical parameters. At the result of their study, comparing the HSA results with those obtained using genetic algorithm (GA) revealed that the HSA can converge to optimum solution with higher accuracy.

Turgut, et al. (2014) investigated the thermal design of shell and tube heat exchangers by using Improved Intelligent Tuned Harmony Search (I-ITHS) algorithm. In their study, they aimed that increase the search capacity of the ITHS algorithm by using chaotic

sequences, and applying alternate search strategies obtained by Artificial Bee Colony algorithm and Opposition Based Learning to promising territories. In addition, Design variables including baffle spacing, shell diameter, tube outer diameter and number of tube passes are used to minimize the total cost of heat exchanger that incorporate capital investment and the total discounted annual energy expenditures related to pumping and heat exchanger area. Results show that I-ITHS is capable to utilized in optimizing STHE.

Vahdat Azad et al. (2016) analyzed the application of nanofluid to increase the efficiency of heat exchangers while declining energy consumption and overall cost. At their study, alumina was used as an appropriate nanofluid. At the consequence of their investigation, they revealed the result that Alumina nanofluid raises the Nusselt number. Therefore, the heat transfer coefficient of shell and tube heat exchangers was increased by nanofluid. Obtained heat transfer coefficients decreased the tube length being required leading to reduced pressure drop in the heat exchanger. In addition, over 185% raising in tube side heat transfer coefficient makes possible declination of heat exchanger length and flow velocity and hance, declining of pressure drop up to 94% and the overall cost of the heat exchanger decreased more than 55%.

Farajollahi et al. (2010) stated that the efficacy of Peclet number, volume concentration of suspended nanoparticles, and particle type on the heat characteristics. For the process, heat transfer characteristics of γ - Al2O3 / water and TiO2 / water nanofluids in a STHE under turbulent flow condition, measured and compared each other. At the consequence of investigation, Crosscheck of the heat transfer behavior of two nanofluids showed that at a certain Peclet number, heat transfer characteristics of TiO_2 / water nanofluid at its optimum nanoparticle concentration level were higher than those of γ - Al_2O_3 / water nanofluid while γ - Al_2O_3 / water nanofluid possessed better heat transfer behavior at greater nanoparticle concentrations.

Arani and Moradi (2019) examined the fluid flow and heat transfer of water inside the segmental baffle shell and tube heat exchanger (SB-STHE) optimization according to 2 different baffle types, including disk baffle (DB) and combined segmental-disk baffle (CSDB). Then, they combined baffle and longitudinally ribbed tube configuration and applied to study the thermohydraulic behavior of STHE with the new baffles and ribbed tube in a 3D geometry. Collected experimental data and numerical results available in the literature were collected and obtained results were compared with them. As a result of their

research, they revealed that the pressure drop reduces due to the directional movement of the fluid along the axis of the tubes. Obtained data of their study showed that the DB-STHE and CSDB-STHE considerably reduced the shell side pressure drop rather than common SB-STHE. With new tubes, heat transfer also enhanced due to the promoting area of heat exchanging with this ribbed tube. According to obtained results, among the proposed combinations, the disk baffle showed the best performance the compare with other combinations.

Sadeghzadeh et al. (2015) optimized a finned STHE utilizing a non-dominated sorting genetic algorithm (NSGA-II). In addition, they compared the results towards a one-objective algorithm to obtain the best solutions. Their research considered nine parameters including: tube arrangement, tube diameter, tube pitch, tube length, number of tubes, fin height, fin thickness, baffle spacing ratio, and number of fins per unit length of the tube. Additionally, they used the "Delaware modified" technique to define heat transfer coefficients and pressure drop of shell-side by considering the baffle cut is 20 percent and the baffle ratio limits range from 0.2 to 0.4. At the end of their research, they observed that the heat transfer rate wander from 3517 to 7075 kW. In addition, variations of shell-side pressure drop with total cost depicted that the pressure drop wander from 3.8 to 46.7 kPa.

Fettaka et al. (2013) used a multi-objective optimization of the heat transfer area and pumping power of a STHE within multiple Pareto-optimal solutions which capture the trade-off between the two objectives by considering nine parameters; tube layout pattern, number of tube passes, baffle spacing, baffle cut, tube-to-baffle diametrical clearance, shell-to-baffle diametrical clearance, tube length, tube outer diameter, and tube wall thickness. They performed the optimization in two case studies from the open literature are presented by using the fast and elitist non-dominated sorting genetic algorithm (NSGA-II) available in the multi-objective genetic algorithm module of MATLAB. As a result of their optimization, they obtained those better values of the two objective functions than the ones previously published. The costs for optimal design were lower than those reported in the literature for both case studies. In addition, they demonstrated the resulting impact of using continuous values of the tube length, diameter and thickness cause that using continuous values of these three decision variables only leads to marginally improved performance compared to discrete values.

Lotfi et al. (2012) tested heat transfer enhancement of multi-walled carbon nanotube (MWNT)/water nanofluid in a horizontal shell and tube heat exchanger. At their study, they obtained carbon nanotubes by the use of catalytic chemical vapor deposition (CCVD) method. Co–Mo / MgO components are used as nano-catalyst for this process. The result that the heat transfer enhances in the presence of multi-walled nanotubes in comparison with the base fluid, was revealed.

Alazwari and Safaei (2021) investigated the thermal performance and flow characteristics of a STHE with several baffle angles. They operated the heat exchanger with distilled water and a hybrid nanofluid at three concentrations of GNP-Ag/water. In their study, they kept the ratio of GNP and Ag at 0.04% and 0.10% respectively. Additionally, they ranged Reynolds numbers between 10,000 and 20,000, whilst baffle angles were set at 45°, 90°, 135°, and 180°. At Re = 20,000, they obtained that the Nu number was the greatest with 35% according to reference case, belonging to a baffle angle of 135°. Also, their results related to friction factor and pressure drop revealed that more locations with fluid blocking were occurred by rising the baffle angle, resulting in increased pressure drop value and friction. The consequent of the temperature streamlines counter, they concluded that the best baffle angle was 135° which maximum heat removal and they observed the best thermal performance.

Patel et al. (2021) explored the quantitative comparative analysis of nine recently developed optimization algorithms for the economic optimization of the heat exchangers. In their study, they considered nine algorithms including Passing Vehicle Search, Salp Swarm Algorithm, Artificial Fora Optimization, Grey Wolf Optimizer, Electro-Search Algorithm, Grasshopper Optimization Algorithm, Symbiotic Organisms Search, Ant Lion Optimizer, and Heat Transfer Search Algorithm. Additionally, they optimized three different heat exchangers including shell and tube, plate-fin, and fin-tube heat exchangers. In study, firstly, statistical analyses of the results were applied to determine the importance between the results of comparative algorithms. The effect of various constraint techniques on the performance of the algorithms were identified. After that, they presented the optimized economically geometry of each of the heat exchanger, and finally, they determined that the convergence of the considered algorithm in obtaining the minimum total cost solutions. the consequent of their study was that; they explored that GOA and SOS algorithms converged to the optimum solution than other competitive algorithms. Additionally, they concluded

from their study that presented optimization algorithms can be experimented to addressed other applied optimization problems.

3. MATERIAL AND METHOD

3.1. Definition of the Problem

The heat exchanger design problem that will be tested at metaheuristic algorithm, is composed by considering TEMA E type STHE obtained from litrature (Shah and Sekulic, 2003). One example of Type E model is illustrated in Figure 3.1. In this thesis, fifteen different values that affect the total cost of heat exchanger, are determined. Then AVOA is generated to calculate the optimized values of fifteen valuables. It also should be considered for the design problem taken from literature that; the problem is improved by changing the tube fluids as nanofluids in stead of sea water. The models that include nanofluid solitons require more calculation to determine thermophysical parameters of solution like heat capacity, density, thermal conductivity, viscosity. Therefore, overall heat transfer and total heat transfer rate can be determined correctly.

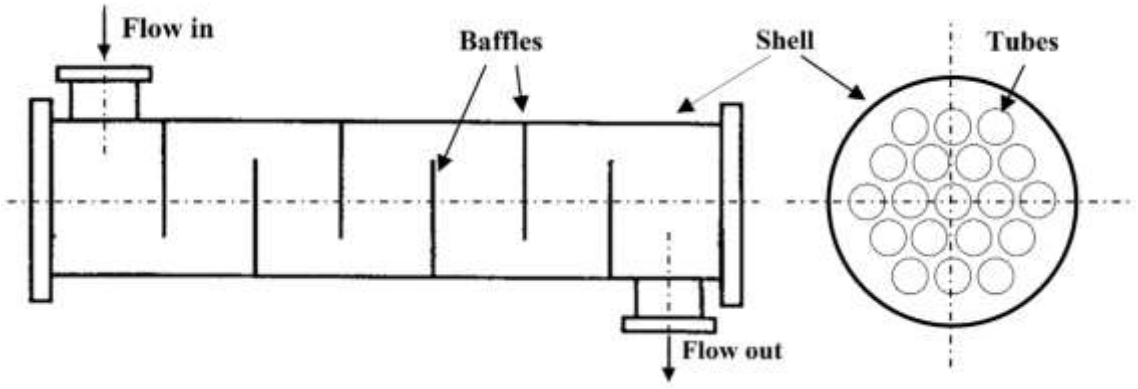

Figure 3.1. A model of Type E STHE.

3.2. Matematical Modeling of Shell and Tube Heat Exchanger

3.2.1. Mathematical Formulation of Heat Transfer

Total heat transfer rate based on heat exchanger effectiveness is calculated by Eq. 1 (Shah and Sekuli, 2003);

$$Q = \varepsilon . C_{\min} . (T_{s,i} - T_{t,i}) \tag{1}$$

where $C_{\min}$ represents the minor value between shell and tube side heat capacities; $T_{s,i}$ is shell side inlet temperatures; $T_{t,i}$ is temperature in tube side and ε represents the heat exchanger effectiveness. The formulation of heat exchanger effectiveness can be obtained from Table 3.1 for TEMA E type STHE used in this case.

Table 3.1. ε–NTU Formulas and Limiting Values of e for C* = 1 and NTU → ∞ for Various Exchanger Flow Arrangements (Shah and Sekulic, 2003).

Flow Arrangement	ε-NTU Formulas	ε-NTU Formulas for $C^* = 1$	Asymptotic Value of ε When NTU → ∞
Counterflow	$\varepsilon = \dfrac{1-\exp[-\mathrm{NTU}(1-C^*)]}{1-C^*\exp[-\mathrm{NTU}(1-C^*)]}$	$\varepsilon = \dfrac{\mathrm{NTU}}{1+\mathrm{NTU}}$	$\varepsilon = 1$ fop all C^*
Parallelflow	$\varepsilon = \dfrac{1-\exp[-\mathrm{NTU}(1+C^*)]}{1+C^*}$	$\varepsilon = \frac{1}{2}[1-\exp(-\mathrm{NTU})]$	$\varepsilon = \dfrac{1}{1+C^*}$
Crossflow, both fluids unmixed	$\varepsilon = 1-\exp(-\mathrm{NTU}) - \exp[-(1+C^*)\mathrm{NTU}]\sum_{n=1}^{\infty} C^{*n} P_n(\mathrm{NTU})$ $P_n(y) = \dfrac{1}{(n+1)!}\sum_{j=1}^{n}\dfrac{(n+1-j)}{j!}y^{n+j}$	Same as general formula with $C^* = 1$	$\varepsilon = 1$ for all C^*
Crossflow, one fluid mixed, other unmixed	For $C_{\min}$ mixed, $C_{\max}$ unmixed, $\varepsilon = 1-\exp\{-[1-\exp(-\mathrm{NTU}\cdot C^*)]/C^*\}$	$\varepsilon = 1-\exp\{-[1-\exp(-\mathrm{NTU})]\}$	For $C_{\max}$ mixed, $\varepsilon = 1-\exp(-1/C^*)$
Crossflow, both fluids mixed	For $C_{\max}$ mixed, $C_{\min}$ unmixed, $\varepsilon = \dfrac{1}{C^*}(1-\exp\{-C^*[1-\exp(-\mathrm{NTU})]\})$ $\varepsilon = \dfrac{1}{\dfrac{1}{1-\exp(-\mathrm{NTU})} + \dfrac{C^*}{1-\exp(-\mathrm{NTU}\cdot C^*)} - \dfrac{1}{\mathrm{NTU}}}$	$\varepsilon = \dfrac{1}{2/[1-\exp(-\mathrm{NTU})] - 1/\mathrm{NTU}}$	For $C_{\max}$ mixed, $\varepsilon = [1-\exp(-C^*)]/C^*$ $\varepsilon = \dfrac{1}{1+C^*}$
1–2 shell-and-tube exchanger; shell fluid mixed; TEMA E shell	$\varepsilon = \dfrac{2}{(1+C^*)+(1+C^{*2})^{1/2}\coth(\Gamma/2)}$ where $\Gamma = \mathrm{NTU}(1+C^{*2})^{1/2}$ $\coth(\Gamma/2) = (1+e^{-\Gamma})/(1-e^{-\Gamma})$	$\varepsilon = \dfrac{2}{2+\sqrt{2}\coth(\Gamma/2)}$ where $\Gamma = \sqrt{2}\,\mathrm{NTU}$	$\varepsilon = \dfrac{2}{(1+C^*)+(1+C^{*2})^{1/2}}$

Aforementioned NTU and C^* in Table 3.1, are abbreviations of the number of heat transfer units and the ratio between $C_{\min}$ and $C_{\max}$ respectively. NTU can be determined by using Eq. 2;

$$NTU = \frac{U_o A_o}{C_{\min}} \tag{2}$$

In the above Eq. 3, A_o presents the total heat transfer area. A_o is calculated by;

$$A_o = N_t \,.\, \pi \,.\, d_o \,.\, L_t \tag{3}$$

where L_t is the total tube length and N_t represents the number of tubes in the tube bundle obtained by empirical equation;

$$N_t = C\left(\frac{D_s}{d_o}\right)^{n_1} \tag{4}$$

C and n_1 are constant empirical parameters and they are defined according to tube arrangement and the number of tube passes. Tabular values of these parameters are indicated in Table 3.2;

Table 3.2. Model parameters for the computition of tube diameter (Fettaka et al., 2013).

Number of Tube Passes	Triangular pitch		Square pitch	
	C	n_1	**C**	n_1
1	0.319	2.142	0.215	2.207
2	0.249	2.207	0.156	2.291
4	0.175	2.285	0.158	2.263
6	0.0743	2.499	0.0402	2.617
8	0.0365	2.675	0.0331	2.643

The overall heat transfer coefficient can be obtained by (Shah and Sekuli, 2003);

$$U_o = \frac{1}{\frac{1}{h_s} + R_{o,f} + \frac{d_o \ln(d_o / d_i)}{2k_w} + R_{i,f}\frac{d_o}{d_i} + \frac{1}{h_t}\frac{d_o}{d_i}} \tag{5}$$

$$d_i = d_o - thck \tag{6}$$

where $R_{o,f}$ and $R_{i,f}$ are shell and tube side fouling factor respectively; d_o is outer diameter and d_i inner tube diameters and it is calculated with Eq. 6; h_s and h_t are shell and tube side heat transfer coefficient; k_w indicates the thermal conductivity of the tube wall. In Equation 6, $thck$ represents the thickness of tubes.

3.2.2. Tube Side Heat Transfer Coefficient

In this study case, the properties of fluids in tube side show differences on the ground that multiple nanofluids are examined. For this reason, the value of parameters including heat capacity, density, thermal conductivity, viscosity that plays a decisive role to define heat transfer coefficient, pressure drop and Nusselt number is determined before the calculation of tube side paremeters. It should be considered that thermophysical properties of nanofluids is calculated based on mean bulk temperature of nanofluids. Tube side heat transfer coefficient (h_t) demonstrated Eq. 5 is obtained by using Nusselt number of nanofluids that is shown at Equation 7 (Ghozatloo *et al.*, 2014);

$$Nu_{nf} = \frac{h_t d_i}{k_{nf}} \tag{7}$$

$$Nu_{nf} = 0.023.\mathrm{Re}_t^{0.8}.\mathrm{Pr}_t^{0.4} \tag{8}$$

where Nu_{nf} is Nusselt number of nanofluids and can be calculated Dittus-Boelter equation (Eq. 8) (Kakaç and Liu, 2002). Tube side Reynold and Prandtl numbers are estimated by;

$$\mathrm{Re}_t = \frac{\dot{m}_t d_i}{A_{o,t}.\mu_{eff}} \tag{9}$$

and Prandtl numbers can be determined by;

$$\mathrm{Pr}_t = \frac{\mu_{nf}(C_p)_{nf}}{k_{nf}} \tag{10}$$

d_i is the inner tube diameter mentioned Eq. 6, $A_{o,t}$ presents the tube side total heat transfer area, k_{nf} represents the effective thermal conductivity of nanofluids can be computed by using following equation (Anitha *et al.*, 2019)

$$k_{nf} = \frac{k_{bf}(k_{np} + 2k_{bf} + 2(k_{np} - k_{bf})\varphi_v)}{k_{np} + 2k_{bf} - (k_{np} - k_{bf})\varphi_v} \tag{11}$$

where k_{bf} represents the thermal conductivity of base fluid, k_{np} is the thermal conductivity of nano particles and φ_v demonstrates the volume concentration of the solid particles. $(C_p)_{nf}$ in Eq. 10 is the effective specific heat of the nanofluids and is given Eq. 12 (Anitha *et al.*, 2019);

$$(C_p)_{nf} = \left(\frac{\rho_{bf}(1 - f_i)(C_p)_{bf}}{\rho_{nf}}\right) + \left(\frac{\rho_{np} f_i (C_p)_{np}}{\rho_{nf}}\right) \tag{12}$$

where $(C_p)_{bf}$ and $(C_p)_{np}$ are the specific heat of base fluid and nanoparticles respectively. Additionally, ρ_{nf} represents the effective density of nanofluids and the calculation of this parameters is given Eq. 12 (Anitha *et al.*, 2019);

$$\rho_{nf} = (1 - \varphi_v)\rho_f + \varphi_v \rho_p \tag{13}$$

where ρ_f and ρ_p are the density of base fluid and nanoparticles respectively. In Eq. 10, one of the parameters that is required to calculate Prandtl numbers is the effective viscosity of nanofluid (μ_{nf}). The effective viscosity of nanofluid is acquired by following equation (Ghozatloo *et al.*, 2014);

$$\mu_{nf} = \mu_{bf}(1 + 2.5\varphi_v) \tag{14}$$

where μ_{bf} demonstrates the viscosity of base fluids.

3.2.3. Shell Side Heat Transfer Coefficient

Heat transfer coefficient is one of the building paremeter to calculate overall heat transfer coefficient (U_o) and hence overall heat transfer rate (Q) mentioned Eq. 1 and 5. Nevertheless, computation techniques indicate differences according to STHE's types and

the data that want to be obtained. In this section, Bell–Delaware method being the one of solution strategies is used at the heat exchanger design problem to calculate shell-side heat transfer coefficient. According to other strategies, Bell–Delaware method considers five different flow streams to account for the respective effects of various leakages. Therefore, conclusion of heat transfer problem is become more reliable and consistent (Shah and Sekuli, 2003). The shell side heat transfer coefficient is expressed by the following equation;

$$h_s = h_{id} J_c J_l J_b J_s J_r \tag{15}$$

where J_c is the correction factor for baffle configuration (baffle cut and spacing); J_l is the correction factor for baffle leakage effects; J_b is the correction factor for bundle and pass partition bypass streams; J_s is the correction factor for larger baffle spacing at the inlet and outlet sections compared to the central baffle spacing. J_r is the correction factor for any adverse temperature gradient buildup in laminar flows. These correction factors and other related component formulations is given in Table 3.3;

Table 3.3. Formulations of the correction for computation of shell side heat transfer coefficient. (Shah and Sekuli, 2003).

Correction Factors C's	Formulas for parameters for Correction Factors
$J_c = 0.55 + 0.72F_c$	Exact formulation of F_c can be found in Ref.
$J_\ell = 0.44(1-r_s) + [1-0.44(1-r_s)]e^{-2.2r_{lm}}$	$r_s = \dfrac{A_{o,sb}}{A_{o,sb}+A_{o,tb}}$; $r_{lm} = \dfrac{A_{o,sb}+A_{o,tb}}{A_{o,cr}}$
$J_b = \begin{cases} 1 & \text{for } N_{ss}^+ \geq 1/2 \\ e^{-C r_b[1-(2N_{ss}^+)^{1/3}]} & \text{for } N_{ss}^+ \leq 1/2 \end{cases}$	$r_b = \dfrac{A_{o,bp}}{A_{o,cr}}$; $N_{ss}^+ = \dfrac{N_{ss}}{N_{r,cc}}$; $\mathbf{C} = \begin{cases} 1.35 & \text{for } \mathrm{Re}_s \leq 100 \\ 1.25 & \text{for } \mathrm{Re}_s > 100 \end{cases}$
$J_s = \dfrac{N_b - 1 + (L_i^+)^{(1-n)} + (L_o^+)^{(1-n)}}{N_b - 1 + L_i^+ + L_o^+}$	$L_i^+ = \dfrac{L_{b,i}}{L_{bc}}$; $L_o^+ = \dfrac{L_{b,o}}{L_{bc}}$ $n = \begin{cases} 0.6 & \text{for turbulent flow} \\ \frac{1}{3} & \text{for laminar flow} \end{cases}$
$J_r = \begin{cases} 1 & \text{for } \mathrm{Re}_s \geq 100 \\ (10/N_{r,c})^{0.18} & \text{for } \mathrm{Re}_s \leq 20 \end{cases}$	$N_{r,c} = N_{r,cc} + N_{r,cw}$ For $20 < \mathrm{Re}_s < 100$, linearly interpolate J_r from two formulas

F_c is the total number of tubes in the crossflow section.
$A_{o,tb}$ and $A_{o,sb}$ are the total tube-to-baffle and the shell-to-baffle leakage area respectively.
$A_{o,cr}$ and $A_{o,bp}$ are the crossflow area and the magnitude of crossflow area for flow bypass.
$L_{b,i}$, $L_{b,o}$ and $L_{b,c}$ are, respectively, baffle spacing at the inlet, outlet and center.
$N_{r,cw}$ and $N_{r,cc}$ are, respectively, the number of tube rows and effective tube rows in crossflow in the window section.
All correlated formulas can be provided in Ref. (Shah and Sekuli, 2003)

h_{id} , in Eq. 15, is ideal heat transfer coefficient for pure crossflow in an ideal tube bank (Kakaç and Liu, 2002) and is computed by;

$$h_{id} = j_i c_{ps} \left(\frac{\dot{m}_s}{A_{o,cr}} \right) \left(\frac{k_s}{c_{ps}\mu_s} \right)^{2/3} \left(\frac{\mu_s}{\mu_{s,w}} \right)^{0.14} \tag{16}$$

where $A_{o,cr}$ is the crossflow area as like mentioned in Table 3.3, and j_i is the Colburn j-factor for an ideal tube bank and the correlation is obtained by the following equation;

$$j_i = a_1 \left(\frac{1.33}{p_t / d_o} \right)^a (\mathrm{Re}_s)^{a_2} \tag{17}$$

where

$$a = \frac{a_3}{1 + 0.14(\mathrm{Re}_s)^{a_4}} \tag{18}$$

a_1, a_2, a_3, and a_4 are model parameters, and they are demonstrated in Table 3.4 , p_t is the tube pitch and Re_s represents the shell side Reynolds number that is calculated by;

$$\mathrm{Re}_s = \frac{\dot{m}_s d_o}{A_{o,cr}\mu_s} \tag{19}$$

Table 3.4. Model parameters for the Colburn factor j and ideal friction factor fid (Fettaka et. al, 2013).

Tube Layout (º)	Reynold Number	a_1	a_2	a_3	a_4	b_1	b_2	b_3	b_4
30	10^5 - 10^4	0.321	−0.388	1.450	0.519	0.372	−0.123	7.00	0.500
	10^4 - 10^3	0.321	−0.388	–	–	0.486	−0.152	–	–
	10^3 - 10^2	0.593	−0.477	–	–	4.570	−0.152	–	–
	10^2 - 10^1	1.360	−0.657	–	–	45.10	−0.973	–	–
	10 >	1.400	−0.657	–	–	48.00	−1.00	–	–
45	10^5 - 10^4	0.370	−0.396	1.930	0.500	0.303	−0.126	6.59	0.520
	10^4 - 10^3	0.370	−0.396	–	–	0.333	−0.136	–	–
	10^3 - 10^2	0.730	−0.500	–	–	3.500	−0.476	–	–
	10^2 - 10^1	0.498	−0.656	–	–	26.20	−0.913	–	–
	10 >	1.550	−0.667	–	–	32.000	−1.000	–	–
90	10^5 - 10^4	0.370	−0.395	1.187	0.370	0.391	−0.148	6.30	0.378
	10^4 - 10^3	0.107	−0.266	–	–	0.0815	0.022	–	–
	10^3 - 10^2	0.408	−0.460	–	–	6.090	−0.602	–	–
	10^2 - 10^1	0.900	−0.631	–	–	32.10	−0.963	–	–
	10 >	0.970	−0.667	–	–	35.00	−1.000	–	–

3.2.4. Shell and Tube Side Pressure Drop

Analogous to shell side heat transfer, the shell-side pressure drop is affected by various leakage and bypass streams in a segmentally baffled exchanger. The total shell side pressure drop is formulated by;

$$\Delta p_s = \Delta p_{cr} + \Delta p_w + \Delta p_{i-o} = (N_b - 1)\Delta p_{b,id}\zeta_b\zeta_\ell + N_b \Delta p_{w,id}\zeta_b$$

$$+2\Delta p_{b,id}\left(1+\frac{N_{r,cw}}{N_{r,cc}}\right)\zeta_b\zeta_s \qquad (20)$$

As it seen in Eq. 20, shell side pressure drop is affected by three variables include pressure drop in the central (crossflow) section, Δp_{cr}; pressure drop in the window area, Δp_w; and pressure drop in the shell-side inlet and outlet sections, Δp_{i-o}. In Equation 20, N_b represents the number of baffles; $\Delta p_{b,id}$ and $\Delta p_{w,id}$ represent pressure drop that occurred in a crossflow between two baffles and pressure drop concerned with one window section. Additionally, the calculation of $\Delta p_{b,id}$ and $\Delta p_{w,id}$ are indicated in Eq. 21 and Eq. 24 respectively;

$$\Delta p_{b,id} = \frac{4 f_{id} G_s^2 N_{r,cc}}{2\rho_s}\left(\frac{\mu_w}{\mu_m}\right)^{0.25} \qquad (21)$$

where f_{id} represents friction factor related to crossflow fluid and it is computed by;

$$f_{id} = b_1\left(\frac{1.33}{p_t/d_o}\right)^b (\mathrm{Re}_s)^{b_2} \qquad (22)$$

where

$$b = \frac{b_3}{1+0.14(\mathrm{Re}_s)^{b_4}} \qquad (23)$$

Table 3.4 gives the coefficients of Eq. 23. As mentioned, pressure drop related with one window section $\Delta p_{w,id}$ is calculated by;

$$\Delta p_{w,id} = \frac{\dot{m}_s^2(2+0.6N_{r,cw})}{2\rho_s A_s A_{o,w}} \qquad (24)$$

where $A_{o,w}$ is the flow area in the window section and Table 3.5 gives the coefficient factors ($\zeta_b, \zeta_l, \zeta_s$) of Eq. 24.

Table 3.5. Bell–Delaware Method - correction factors for pressure drop on the shell side (Shah and Sekuli, 2003).

Correction Factors, ζ's	Formula for Parameters for Correction Factors
$\zeta_b = \begin{cases} \exp\{-\mathbf{D} r_b [1-(2N_{ss}^+)^{1/3}]\} & \text{for } N_{ss}^+ < \frac{1}{2} \\ 1 & \text{for } N_{ss}^+ \geq \frac{1}{2} \end{cases}$	$\mathbf{D} = \begin{cases} 4.5 & \text{for } \mathrm{Re}_s \leq 100 \\ 3.7 & \text{for } \mathrm{Re}_s > 100 \end{cases}$
$\zeta_l = \exp[-1.33(1+r_s) r_{lm}^p]$	$p = [-0.15(1+r_s)+0.8]$
$\zeta_s = \left(\frac{L_{b,c}}{L_{b,o}}\right)^{2-n'} + \left(\frac{L_{b,c}}{L_{b,i}}\right)^{2-n'}$	$n' = \begin{cases} 1.0 & \text{for laminar flow} \\ 0.2 & \text{for turbulent flow} \end{cases}$

r_b, r_s, r_{lm} and N_{ss}^+ are defined in Table 3.3

The tube side pressure drop can be calculated with (Shah and Sekuli, 2003);

$$\Delta p_t = \frac{\dot{m}_t}{2.\rho_{nf} A_{o,t}^2}\left[\frac{4.f.L}{d_i} + (1-\sigma^2+K_c) - (1-\sigma^2-K_e)\right] n_p \qquad (25)$$

where K_e and K_c are sudden expansion and sudden contraction coefficients, σ is a function of the contraction ratio (Shah and Sekuli, 2003), n_p is the number of tube passes and f is the fanning friction factor, computed by model;

$$f = 0.046\,\mathrm{Re}_t^{-0.2} \qquad (26)$$

3.2.5. Defining The Objective Function

Total cost of heat exchanger (C_{tot}) which used in the study case, is tackled as a problem objective to be optimized by the proposed method. The formulation of C_{tot} is given Eq. 27.

$$C_{tot} = C_i + C_{oD} \tag{27}$$

where C_i represents the capital investment, and is obtained by means of the Hall equation (Taal *et al.*, 2003);

$$C_i = 8000 + 2A_o^{0.93} \tag{28}$$

where A_o, is the total heat transfer area defined in Eq. 3.

C_{oD} represents total discounted operating cost, and is calculated by using following equation;

$$C_{oD} = \sum_{j=1}^{ny} \frac{C_o}{(1+i)^j} \tag{29}$$

where *i* represents the annual discount rate, *ny* is the number of active years of heat exchanger, C_o represents the annual operating cost and is calculated by (Turgut *et. al.*, 2020);

$$C_o = PP.C_E.H \tag{30}$$

C_E represents the energy cost in €/kWh and *H* is the annual amount of operating hours, *PP* is the overall pumping power. The equation of the overall pumping power is given with Eq. 31 (Turgut *et. al.*, 2020);

$$PP = \frac{1}{\eta}\left(\frac{m_t}{\rho_t}\Delta P_t + \frac{m_s}{\rho_s}\Delta P_s\right) \tag{31}$$

3.3. Vulture Species and African Vultures

Before peruse mathematical modelling of AVOA, Vultures; especially African Vultures that inspired algorithm should be examined to comprehend how it works and understand process connections.

Vultures are predatory birds classificated as scavengers, in nature (Ruxton and Houston, 2004). This creature is known by people from almost all regions. One of the biggest reasons is that vultures live in the continents of Asia, Europe, and Africa, where the human population is high. In addition, the vulture species called new world vultures, are also seen in America. The physical anatomy of vultures is one of the essential features that aid to define vultures from other birds. These species are considered to have a bald head and long wingspan, although, it is known some vultures speciate have no bald head. Vulture's bald heads have vital importance for these creatures. Vultures have been observed to open their wings and stretch their necks for lowering body temperature via head skin, in the heat and hunch their bodies and tuck in their heads to preserve their body temperature, in the cold (Arad and Bernstein, 1988).

As it is said in the first paragraph, although vultures are in scavenger species and eat dead animals, it is normative that vultures attack severely wounded, injured, and sick animals. As a result of some observations, vultures also attack healthy animals although very rarely. It has also been observed that some vultures wait for other scavengers to tear the skin if the skin of the dead animal is too thick for the vulture to pierce (Vulture Facts, 2011). Vultures are of great importance for human beings and the ecosystem.

First of all, vultures are one of nature's sweepers. Additionally, they have an active role at places where other scavengers and most predators cannot reach. Besides, Vultures accelerates the transition of creatures to the next step in the cycle of nature, by pointing the dead body to other animals. Their importance to humans is almost the same as other scavengers. Dead bodies or wounded creatures carry many types of bacteria. Also, these places are available places for bacterium and virus mutation and these mutations can be transformed into plagues epidemic which it is really hard to deal with for human beings. Similar plagues have appeared in history like The Black Death (bubonic plagues) or Leprosy (Parıldar, 2020). However, thanks to scavengers such as vultures, many such situations are avoided.

3.3.1. African Vultures; Species, Hunting and Flight Behavior That Inspired AVOA

There are many species of vulture in Africa and each type has special abilities to survive and hunt. According to Houston's works in 1974 (Houston, 1974), African vultures can be evaluated in three classes. While the first class consists of little size vultures that have a small beak like Hooded (Necrosyrtes monachus) and Egyptian (Neophron percnopterus), the vultures in the second class consists of large vultures with strong tearing beaks like Lappet-faced (Torgos tracheliotus) and white-headed (Trigonoceps occipitalis). The third class, on the other hand, consists of the most numerous of the vulture species, and the two griffon species, the white-backed (Gyps ajZcanus) and the larger Ruppell's griffon (Gyps ruppellii) can be given as examples for the third class.

All species of vultures have high visual ability. Besides, these creatures can identify the sick or injured among the group. On the other hand, if the population of creatures is compared with the amount of dead, sick, or wounded animals, finding food for vultures can be very difficult in the natural environment. For this reason, vultures spend most of their lives looking for food. Vultures carefully view their territory for a long time and travel long spans to find for food (Xue *et al.*, 2018). Having energy has vital importance for vultures. A vulture must have high energy to search and fly longer. Given this situation, a satiated vulture has high energy. Nevertheless, as a vulture gets hungry, this instinctively makes this vulture even more aggressive. This condition orientates vulture to the following situation that is one of easier way instead of spending energy looking for food; Vultures don't just fly in search of food. They also look for other vulture species that are already finding food. Possible encounters may cause conflict among two or more than two groups of vultures for one food source (Bosè and Sarrazin, 2007).

As a familiar from a lot of movies and cartoons, vultures generally fly around their hunts, flight behavior of vultures is not only for hunting first, also is used for to distract high-powered vultures to snatch food from them. When a vulture's flight habit is observed, it is seen that vultures constantly fly rotationally used to model of Circular Motion or Spiral Motion. As might be expected, generally, high-powered vultures can find more food because of their ability to fly for a long time. When a group of vultures find food, other groups approach the group has food as Spiral motion. High-powered vultures try to keep their food as far away from other groups as possible. On the other hand, low-powered

vultures surround high-powered vultures and provoke and distract them to make them tired. Therefore, low-powered vultures may get a chance to steal food from high-powered vultures. In this case, starving causes vultures to become more and more aggressive (Bosè and Sarrazin, 2007; Kendall *et al.*, 2012).

3.4. African Vulture Optimization Algorithm (AVOA)

Section 3.3, it is described how the African Vulture behaves. Considering the habit of African Vultures, the best course of action can be summarized as follows for AVOA;

a. There are many species of vulture in Africa and each type has special abilities to survive and hunt.

b. Some species count as high-powered vultures, while others count as low-powered.

c. A satiated vulture has high energy to search and fly longer.

d. Starving causes vultures to become more aggressive

e. Low-powered vultures are also look for other vulture species that are already finding food

f. Vultures constantly fly rotationally used to model of Circular Motion or Spiral Motion.

g. A group of vultures has food, other groups approach the group has food as Spiral motion.

h. Low-powered vultures surround high-powered vultures and provoke and distract them to make them tired

In AVOA, the behavior of African Vultures is simulated by considering the clauses given above. It should be considered that all metaheuristic algorithms on formulation and simulation, contain assumptions about the natural environment.

Initialization of Algorithm

At the beginning of algorithm, N vultures can be found in the default environment; “N” number presents vulture population of African Vulture in AVOA, number N can be increased of decreased according to complexity of the problem to be solved.

As it is mentioned at clauses a and b, vultures are diverse in environment. On the other hand, it is arranged that there are only two groups of vultures in algorithm. After determining the N number that is population in environment, Fitness of the solution values is calculated and the best and second-best solutions are determined. Then the best solution and second-best solution are appointed as the best vulture of first group and the best vulture of second group respectively. Other solutions are programmed to move to best and second-best solution by using Eq. 32. For each iteration, solutions are updated via this process.

$$R(i) = \begin{cases} BestVulture_1 if p_i = L_1 \\ BestVulture_2 if p_i = L_2 \end{cases} \quad (32)$$

In Eq. 32, L_1 and L_2 are parameters calculated before searching and between 0 and 1. In addition, the aggregate of both numbers is 1. The probability of choosing the best solution is gained using the Roulette wheel to choose each of the best solutions for each group using Eq. 33. (Abdollahzadeh B. *et al.,* 2021)

$$p_i = \frac{F_i}{\sum_{i=1}^{n} F_i} \quad (33)$$

In AVOA, if the α-numeric parameter is near to 1 and the β-numeric parameter is near to 0, it will cause an increased concentration. In the opposite case; that is, If the β-numeric parameter is near to 1 and the α-numeric parameter is near to 0, it causes accumulated diversity in AVOA.

The Physical Conditions of African Vultures

As it is mentioned at clauses c and d, a satiated vulture has high energy and it can fly longer in search of food. When it is considered clause c and d, it can be inferred that state of hunger makes vultures more aggressive. This physical condition of vultures is called "saturation state" and it represents the rate of vultures being satiated. The saturation state is modeled in AVOA by using Eq. 34. (Abdollahzadeh B. *et al.,* 2021);

$$F = (2 \times rand_1 + 1) \times z \times \left(1 - \frac{iter_i}{\max iter}\right) + t \quad (34)$$

In Eq. 34 F represents saturation state, $iter_i$ represents the current number of in iteration, $\max iter$ represents the total iteration number. Besides, $rand_1$ is a random number between 0 and 1, z is a random number between -1 and 1, it shows the alteration for each

iteration. If number z drops below 0 , it shows that the vulture is starving; in the opposite case; that is, if number z goes above 0 , it means the vulture is hungry.

t in Eq. 34 is used to improve the performance in solving complex optimization problems that increase the credibility of escaping from local optimal points and it illustrated in Eq. 35 (Jia *et al.*, 2019).

$$t = h \times \left(\sin^{w} \left(\frac{\pi}{2} \times \frac{iter_i}{\max iter} \right) + \cos \left(\frac{\pi}{2} \times \frac{iter_i}{\max iter} \right) - 1 \right) \tag{35}$$

In Eq 4, h presents a random number between -2 and 2. w presents the parameter with a fixed number arranged before the optimization operation, and w indicates the optimization operation disrupts the exploration and operation phases. As the value of w raises, the likelihood of inserting the exploration phase during the final optimization phases raises, in the opposite case; that is, as the value of w regress, the likelihood of entering the exploration phase decreases.

The state of hunger plays a key role not only for the saturation state but also for the act of aggression and consequent aggression. In some of the iterations in AVOA, Eq. 34 and Eq. 35 perform saturation, that is, exploration, while in some iterations, they perform food stealing, that is, exploitation. The main goal of this strategy is to change Eq. 35 to modify the discovery and exploit phases so that at some point in the AVOA optimization process it can enhance the prospect of inserting the exploration phase.(Jia *et al.*, 2019)

If value |F| more than 1, vultures look for food on variable territories and AVOA inserts exploration phase. If value |F| less than 1, AVOA inserts exploitation phase and vultures seek food around vultures being close the best solution.

Exploration

In AVOA, vultures examine various areas. It can be used two different strategies in algorithm. It is used P_1 parameter to determine strategy in process; P_1 taking values between 0 and 1, creates range of use strategies. This parameter is evaluated before examination process.

In exploration phase, a random number called $rand_{P1}$ is generated in the range of 0 to 1. Then number $rand_{P1}$ and parameter P_1 are compared to determine the strategy that will use. The equation about this process illustrated in Eq. 36.

$$P(i+1)=\begin{cases} Equation(37) if P_1 \geq rand_{P1} \\ Equation(39) if P_1 < rand_{P1} \end{cases} \quad (36)$$

As it seen in Eq. 36, if the value $rand_{P1}$ is equal or more than the value P_1, Eq. 37 is used. However, if the value $rand_{P1}$ is less than the value P_1, Eq. 39 is used. In this case, each vulture searches randomly in the environment according to the saturation parameter F. The Eq. 37 is mentioned in Eq. 36 and its strategy are given below (Abdollahzadeh B. *et al.,* 2021).

$$P(i+1)=R(i)-D(i)\times F \quad (37)$$

In Equation 37; The vultures randomly search the area for food, with the best of both initially identified groups ($BestVulture_1$ and $BestVulture_2$) at a random distance among them. In Eq. 37, $P(i+1)$ presents the location vector of vultures in subsequent iteration. F presents the rate of vultures being satiated that is revealed by using Eq. 35. $D(i)$ used in Eq. 37 is indicated in Eq. 38 (Abdollahzadeh B. *et al.,* 2021).

$$D(i)=|X\times R(i)-P(i)| \quad (38)$$

In Eq. 38, $R(i)$ is one of the best vultures in current iteration chosen by using Eq. 32. X is where vultures move randomly to safeguard food from other vultures. X is used as a coefficient vector that increased random motion and that shows difference each iteration. In addition, X is obtained by using equation; X = 2 x $rand$. In this equation $rand$ is a random number between 0 and 1. $P(i)$ represents the position of the current vector of the vulture.

Other strategy Eq. 39 is mentioned in Eq. 36 and its strategy are given below (Abdollahzadeh B. *et al.,* 2021).

$$P(i+1)=R(i)-F+rand_2\times((ub-lb)\times rand_3+lb) \quad (39)$$

In Eq. 39, $R(i)$, as in Equations 37 and 38, is one of the best vultures in current iteration chosen by using Eq. 32. Likewise, F is the rate of vultures being satiated that is obtained by using Eq. 35. $rand_2$ is random number between 0 and 1. lb and ub represent lower and upper boundaries.

By using strategy given in Eq. 39, Model is acquired to obtain random solution between ub and lb. $rand_3$ is operated to increase random nature coefficient. It $rand_3$

receive a value close to 1, the solutions are distributed parallel patterns, and this situation suffixes a random motion along with the lb. It creates a high random coefficient at the range of search environment to raise variety and search for different search territories. It should be considered that the simplest models are used to model vultures' motions in AVOA.

Exploitation (Approach)

As it is mentioned at clauses h, a vulture which has trouble finding food and which struggle with hunger, moves to vultures that have already found food to steal from them. This behavior is called "Exploitation". In AVOA, when the saturation state value, |F|, is at between 0.5 and 1, it means that algorithm enters exploitation approach phase. This phase actualizes 2 different strategies called "competition strategy" and "rotary flight strategy". Determination of the strategy is evaluated with P_2 parameter. At the beginning of process, it is created a random value called $rand_{P2}$ being between 0 and 1. Then algorithm compares $rand_{P2}$ and P_2 to determine strategy. If the value $rand_{P2}$ is equal or more than the value P_2, competition strategy is activated. However, if the value $rand_{P2}$ is less than the value P_2, rotary flight strategy is activated. The Equation about this process is given Eq. 40.

$$P(i+1) = \begin{cases} Equation(41) if P_2 \geq rand_{P2} \\ Equation(44) if P_2 < rand_{P2} \end{cases} \quad (40)$$

When clause h is considered, it is also made inference that lack of food cause conflicts among vultures. If the equation |F| > 0.5 is satisfied, the vulture has sufficient energy and are relatively satiated. In algorithm, these vultures are accepted as high-powered vultures and they are successful seekers for food. However, they will not have tolerance sharing food with other vultures. On the other hand, low-powered vultures gather around high-powered vultures and they try to steal food from them. It also causes conflict between two groups. This behavior is defined as completion strategy in AVOA and it is modeled with Eq. 41 (Abdollahzadeh B. *et al.*, 2021).

$$P(i+1) = D(i) \times (F + rand_4) - (R(i) - P(i)) \quad (41)$$

F and $D(i)$ values are evaluated via Eq. 35, and Eq. 38 respectively. $rand_4$ is a random number between 0 and 1. In addition, it $rand_4$ is used to boost random coefficient. $R(i)$ represents one of the best vultures in current iteration chosen by using Eq. 32. $P(i)$ represents the position of the current vector of the vulture.

In exploitation approach phase, the other strategy is rotary flight strategy. As it is mentioned clause f and g, vultures take a spiral approach through rotation. This Spiral Motion in AVOA and the instance from nature are illustrated Figure 3.2.

When mentioned spiral motion is modelled mathematically, Eq. 42 and Eq. 43 are obtained. The rotary flight strategy can be modeled like Eq. 44 by using Eq. 42 and Eq. 43.

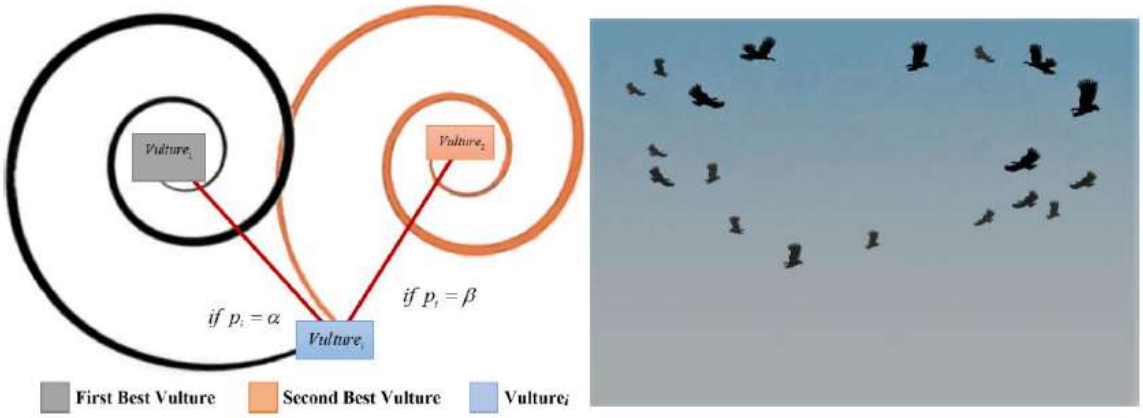

Figure 3.2. Vultures spiral motion (The Emergence Network, 2019).

$$S_1 = R(i) \times \left(\frac{rand_5 \times P(i)}{2\pi} \right) \times \cos(P(i)) \tag{42}$$

$$S_2 = R(i) \times \left(\frac{rand_6 \times P(i)}{2\pi} \right) \times \sin(P(i)) \tag{43}$$

$$P(i+1) = R(i) - (S_1 + S_2) \tag{44}$$

In equations, $R(i)$ is one of the best vultures in current iteration chosen by using Eq. 32. $P(i)$, as in the previous equations, represents the position of the current vector of the vulture. $rand_5$ and $rand_6$ are random numbers between 0 and 1. In AVOA, Equation 44 are obtained by using Eq. 32 and Eq. 43. At the end of process, current locations of vultures are updated according to Eq. 44.

Exploitation (Conflict)

In this phase of exploitation, low-powered vultures gather around food resource which is determined by the best vulture of first group and the best vulture of second group. In

AVOA, when the saturation state value, |F|, is lower than 0.5, it means that algorithm enters exploitation conflict phase and this situation cause to occur two different behavior called "sieges" and "aggressive strife". Determination of the behavior is evaluated with P_3 parameter. At the beginning of process, it is created a random value called $rand_{P3}$ being between 0 and 1. Then algorithm compares $rand_{P3}$ and P_3 to determine behavior. If the value $rand_{P3}$ is equal or more than the value P_3, siege behavior occurs. However, if the value $rand_{P3}$ is less than the value P_3, aggressive strife behavior occurs. The equation about this process is given Eq. 45.

$$P(i+1) = \begin{cases} Equation(48) if P_3 \geq rand_{P3} \\ Equation(49) if P_3 < rand_{P3} \end{cases} \quad (45)$$

The first behavior sieges is mathematical modeling of the movement of all vulture species towards the source food. In the case of starvation, the mathematical modeling of vultures' movement behavior related with the current location of the best first vulture and the best second vulture is given in Eq. 46 and Eq. 47 (Abdollahzadeh B. *et al.,* 2021).

$$A_1 = BestVulture_1(i) - \frac{BestVulture_1(i) \times P(i)}{BestVulture_1(i) - P(i)^2} \times F \quad (46)$$

$$A_2 = BestVulture_2(i) - \frac{BestVulture_2(i) \times P(i)}{BestVulture_2(i) - P(i)^2} \times F \quad (47)$$

In Eq. 46 and Eq. 47, $BestVulture_1(i)$ is the best vulture of first group and $BestVulture_2(i)$ is the best vulture of second group. F represents the rate of vultures being satiated that is obtained by using Eq. 35 and, $P(i)$ represents the position of the current vector of the vultures. The mathematical modeling of gathering around food source that is siege behavior related with Eq. 46 and Eq. 47 is given in Eq. 48.

$$P(i+1) = \frac{A_1 + A_2}{2} \quad (48)$$

In Eq. 48, A_1 and A_1 are acquired by using Eq. 46 and Eq. 47. $P(i+1)$ represents next step location vector of vulture. In exploitation conflict phase, the other behavior is aggressive strife. It occurs when |F| is less than 0.5. Under conditions |F| < 0.5, the vulture is starving and it doesn't have enough energy to conflict high-powered vultures. On the other

hand, there are a lot of low-powered vultures and all low powered vultures move together to best vultures from diverse directions. The mathematical model of aggressive strife behavior is given in Eq. 49 (Abdollahzadeh B. *et al.,* 2021).

$$P(i+1) = R(i) - |d(t)| \times F \times Levy(d) \tag{49}$$

In Eq. 49, $d(t)$ indicates the span between a vulture and one of the best vultures belongs two groups, and it can be calculated by using Eq. 42. $Levy(d)$ in the equation represents the Levy Flight Motion. Levy Flight (LF) is an equation that is capable to increase efficiency in AVOA and that is effectiveness has been defined and used in many studies. LF in Eq. 49 is calculated by using Eq. 50 (Abdollahzadeh B. *et al.,* 2021).

$$Levy(d) = 0.01 \times \frac{u \times \sigma}{|v|^{\frac{1}{\beta}}}, \quad \sigma = \left(\frac{\Gamma(1+\beta) \times \sin\left(\pi\beta/2\right)}{\Gamma(1+\beta 2) \times \beta \times 2\left(\beta - 1/2\right)} \right)^{\frac{1}{\beta}} \tag{50}$$

In Eq. 50, d indicates the dimensions of case, u and v are random numbers between 0 and 1. β is a fixed and default number of 1.5.

3.5. Pseudocode of Study Case

Pseudocode is an informal way of programming description that does not require any strict programming language syntax or underlying technology considerations and it is used for creating an outline or a rough draft of a program. Pseudocode summarizes a program's flow, on the other hand, excludes underlying details. The pseudocode of algorithm which is used this study case is described in Table 3.6;

Table 3.6. Pseudocode of African vulture optimization algorithm.

```
// Initialize algorithm parameters
N = Population size
LowBound = Lower bounds
UpBound =Upper bounds
maxIter = Maximum number of iterations
f(x) = Objective function
Initialize the random population P_i (i = 1,2, ..., N)
Set iteration counter (Iter) to 1
While (Iter < maxIter)
    Calculate the fitness values of Vulture (Vi)
    Set the first-best location as a best vulture for category 1 (P_BestVulture1)
    Set the second-best location as a best vulture for category 2 (P_BestVulture2)
    for i = 1 to N
        Select R(i) using Eq. 32
        Update the F using Eq. 34
        if (|F| ≥ 1)
            if (P1 ≥ randP1)
                Update the location Vi with Eq. 37
            end
        else
            Update the location Vi with Eq. 39
        end
        if (|F| < 1)
            if (|F| ≥ 0.5)
                if (P2 ≥ randP2)
                    Update the location Vi with Eq. 41
                else
                    Update the location Vi with Eq. 44
                end
            else
                if (P3 ≥ randP3)
                    Update the location Vi with Eq. 48
                else
                    Update the location Vi with Eq. 49
                end
            end
        end
        Apply boundary check
        Determine P_BestVulture1
        Iter++
    end
end
Output the location of Vi and its fitness value
```

4. RESULTS AND DISCUSSION

Shell and tube heat exchangers have auxiliary components due to their structural properties, and structural errors may occur during the assembly of these auxiliary elements. In connection with that, structural faults can create alternating flow currents and leakages. As is mentioned in Section 3.2.3, the Bell – Delaware method is the most consummate design strategy among other design strategies in the literature to remove structural errors that arise during the assembly of auxiliary components of the heat exchanger. On the ground the reason stated above, the effectiveness of algorithm in an optimization problem that is restricted with real-world constrained is evaluated by designing a shell and tube heat exchanger by using Bell–Delaware method. A case study taken from the literature (Shah and Sekuli, 2003) study is modified to make compatible STHE formalization for the nanofluid solution. Afterward, the obtained function is adroitly solved with six different particles by AVOA. Acquired solution results are compared among six nanofluids been obtained by mixing with water and a certain amount of Al_2O_3, CuO, TiO_2, Cu, SiO_2, and Boehmite particles. AVOA will be operated to maintain an optimal shell and tube heat exchangers design from a thermo-economic point of view. There are sixteen design variables are defined in this study case to be optimized. N_{ss}, N_{pass}, and T_{layout} are defined as integers in contrast with others.

All variables are prescribed between boundaries given in Table 4.1.

The considered case study carries out with thermodynamical forming of a STHE with an obligatory heat load of 391.3 kW, whose tube side fluids consist of nanofluids and shell side fluid is oil. The main benchmark data, that is, the discounted operating cost values, which are defined in Eq. 29 and Eq. 30, are evaluated with ny = 10 years, annual discount rate I = 10%, energy cost C_E = 0,12 €/kWh and total working hours H = 7000 €/h values, taking into account previous research studies (Mohanty, 2016; Asadi *et al.*, 2014). Table 4.2 gives information about operating conditions and nanofluid properties. Additionally, the properties of nanofluids component, are given in Table 4.3 (Anitha *et al.*, 2019; Clary and Mills, 2011; Jia *et al.*, 2019; Sonawane, *et. al.*, 2015; Żyła and Fal, 2017).

Table 4.1. Upper and lower bounds for STHE (Turgut et. al., 2020).

	Lower bound	**Upper bound**
Shell-side inside diameter - D_s (m)	0.3	0.6
Tube-side outside diameter – d_o(m)	0.012	0.025
Tube length - L (m)	3	10
Tube pitch - p_t (m)	0.015	0.03
Central baffle spacing - L_{bc}(m)	0.2	0.5
Inlet baffle spacing - L_{bi}(m)	0.2	0.5
Outlet baffle spacing - L_{bo} (m)	0.2	0.5
Baffle spacing (%)	15	40
Width of bypass lane - w_p (m)	0.01	0.03
Tube-to-baffle hole diametral clearance - δ_{tb} (m)	0.0001	0.001
Shell-to-baffle diametral clearance - δ_{sb} (m)	0.001	0.005
Tube thickness - *thck* (m)	0.0002	0.002
The nanoparticle ratio – φ_v (%)	0	0.6
Number of tube passes - N_{pass}	1	2 4 6 8
Number of sealing strip pairs - N_{ss}	1	2 4 8
Tube Layout - T_{layout} (°)	30	45 90

Table 4.2. Operating conditions (Turgut et. al., 2020).

Process fluids	Shell Side	Tube Side					
	Oil	**Water – Al_2O_3**	**Water -CuO**	**Water – TiO_2**	**Water -Cu**	**Water – SiO_2**	**Water -Boehmite**
Flow rate (kg/s)	36.3	18.1	18.1	18.1	18.1	18.1	18.1
Inlet Temperature (°C)	65.6	32.2	32.2	32.2	32.2	32.2	32.2
Outlet Temperature (°C)	60.4	37.42	37.42	37.42	37.42	37.42	37.42
Density (kg/m^3)	849	1080.88	1076.56	1114.83	1151.12	1052.49	997.34
Fouling Resistance (m^2 K/ W)	0.000088	0.000176	0.000176	0.000176	0.000176	0.000176	0.000176

Table 4.3. The properties of nanoparticles and base fluid (Anitha et al., 2019; Clary and Mills, 2011; Jia et al., 2019; Sonawane, et. al., 2015; Żyła and Fal, 2017).

Components	Base fluid	Nanoparticles					
	Water	**Al_2O_3**	**CuO**	**TiO_2**	**Cu**	**SiO_2**	**Boehmite**
Density (kg/m^3)	995	-	-	-	-	-	-
Heat capacity (J/kg K)	4178	3970	6000	4250	8933	2220	3050
Viscosity (Pa s)	0.000759	765	551	686	385	745	618.8
Thermal Conductivity (W/m K)	0.619	40	33	8.9	400	1.4	30

The optimization conditions are also restricted to three constraints that are set on the design problem. The first restriction is determined as not allowed more than 50 kPa pressure drop in shell side, and lower than 1.0 kPa in tube side. The second restriction is the thermal surface area of 50 m2 should not be violated. Furthermore, the pitch number should not be higher than 1.25 times of tube-side out diameters. In this study case, 180 independent runs including 30 runs for each nanoparticle are illustrated in Table 4.4;

Table 4.4. The algorithm output of overall cost for each nanoparticle.

	Total Cost (€)					
	Al_2O_3	**CuO**	**TiO_2**	**Cu**	**SiO_2**	**Boehmite**
1	23059.52	22582.03	21504.30	27483.40	24029.96	26287.82
2	23112.92	22509.11	21487.44	24612.22	22295.35	27600.66
3	23434.27	23492.16	26405.07	28290.50	23221.89	27397.31
4	22416.35	21324.13	23120.88	22547.82	23229.68	24796.60
5	22538.70	23659.25	21931.13	22966.00	22450.10	25479.05
6	26750.42	23458.66	22758.67	25414.21	22621.86	29842.72
7	24898.38	28566.02	25777.60	23408.03	21116.83	23383.80
8	22099.91	21334.27	23701.62	23706.72	23573.94	23205.35
9	22701.18	22350.03	21879.60	28063.89	22750.31	24159.47
10	25109.70	23412.14	23134.53	22988.96	22763.82	23270.27
11	22400.79	23494.36	21434.48	23440.46	22843.26	25907.35
12	23236.37	23538.33	26971.89	23499.29	23438.51	23860.70
13	23834.94	21445.88	21764.21	22823.24	21852.01	25602.64
14	21196.11	22281.67	22981.48	25219.46	22710.52	24022.86
15	25343.95	23162.17	22375.95	23204.83	23192.15	25608.40
16	22583.88	26697.28	24045.33	22503.29	23072.62	24975.96
17	23004.53	22350.12	22186.68	27033.92	23859.24	24345.58
18	23833.82	21750.73	24599.56	28694.91	23672.65	23430.87
19	26885.26	23422.86	26975.40	23792.97	23812.77	23424.53
20	24210.51	22598.46	25647.22	25066.74	22019.31	26938.49
21	21715.13	24282.27	21765.33	26671.78	27273.28	27054.48
22	24036.02	24768.98	21842.61	23173.32	22622.94	26578.30
23	23879.85	23413.31	21861.14	26384.80	26781.71	31139.40
24	22899.48	23136.30	22751.85	23722.81	21633.44	23098.17
25	27739.99	23171.91	22530.46	23079.80	24282.06	23542.40
26	23555.80	23037.37	23896.86	22891.13	23132.09	24914.49
27	23805.36	27015.11	27588.97	26594.31	22764.57	22496.24
28	22677.02	21530.24	22311.51	23245.74	21954.47	27751.33
29	26094.19	22673.47	23485.24	26616.16	24722.50	24553.63
30	23381.62	23633.65	21779.29	23351.83	22095.58	23974.65
Average	23747.86	23336.41	23349.88	24683.08	23192.84	25288.12
Max	27739.99	28566.02	27588.97	28694.91	27273.28	31139.40
Min	21196.11	21324.13	21434.48	22503.29	21116.83	22496.24

As it is seen in Table 4.4, also gives information about the highest and lowest values for each nanoparticle and the arithmetic mean value of the obtained data. In this thesis, the minimum values of all particles are evaluated. In this direction, it is seen that while the

lowest total cost value belongs to SiO_2 among the particles, the highest value belongs to Cu. However, for all examined nanoparticles, the minimum value is generally close to each other and the difference between the lowest and the highest value is 1379.41€. Considering all the data, the average cost is generally close to each other. Statistical analysis is performed, and the stability of the data results for AVOA is also measured, before examining the minimum values obtained for each particle and the resulting problem values in this study case. As mentioned before, metaheuristic algorithms cannot provide a clear and precise result, and the results may not always reflect each other. In general, the results obtained from the algorithm are expected to be stable in a certain range and to obtain a value in that range. For this reason, statistical analysis paves the way for the use of more reliable data in terms of future theoretical and practical studies that can be inspired by this study. Bias (Proximity) graphs of the data obtained in AVOA divided into studied nanofluids are shown in the following figures (Figure 4.1 – 4.6). Bias graphs illustrate the distance of statistically obtained data from the mean of that data. These data are used for variance and standard deviation. The square of the projection lengths from the data shown in the tables to the average cost provides the variance. STHE have auxiliary components due to their structural properties, and structural errors may occur during the assembly of these auxiliary elements. In connection with that, structural faults can create alternating flow currents and leakages.

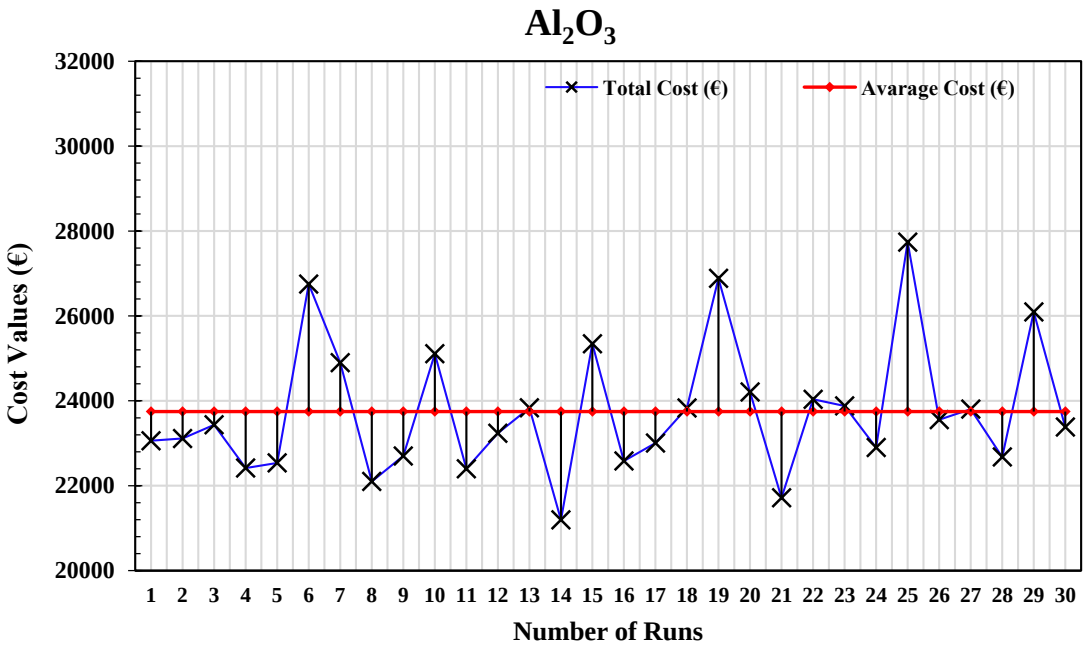

Figure 4.1. Bias (Proximity) graphs of nanofluids based Al_2O_3.

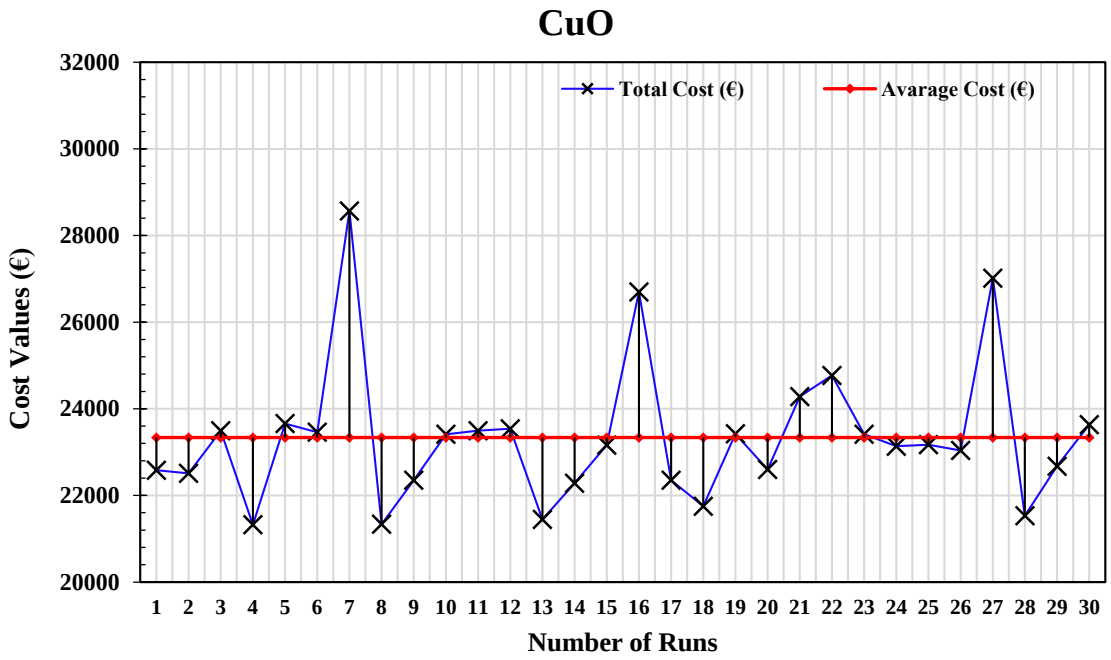

Figure 4.2. Bias (Proximity) graphs of nanofluids based CuO.

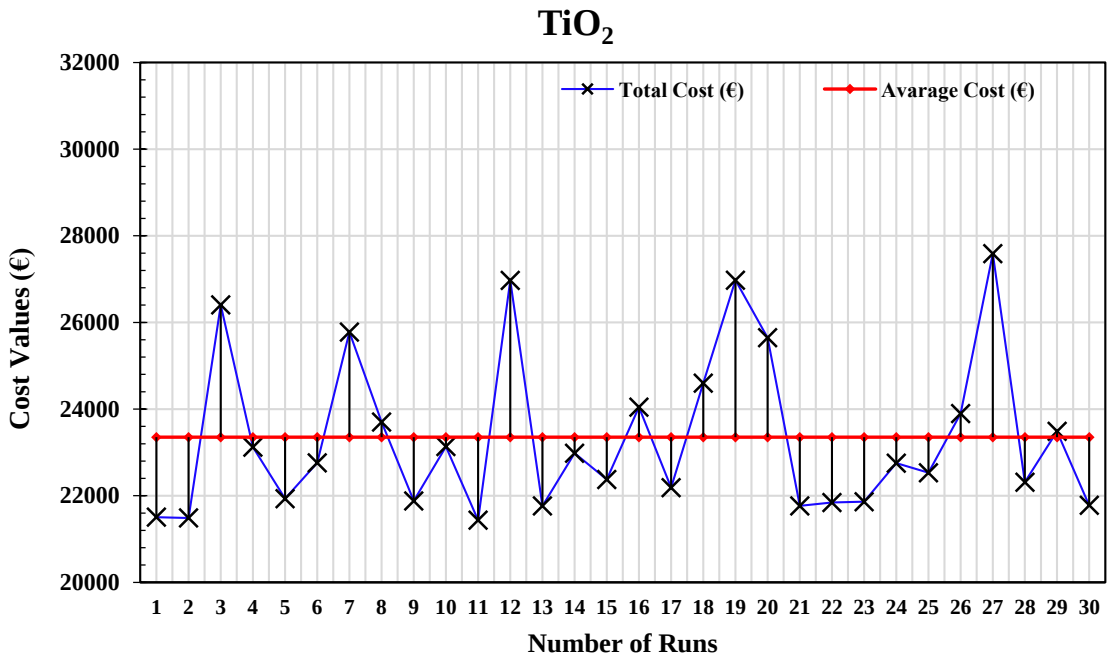

Figure 4.3. Bias (Proximity) graphs of nanofluids based TiO_2.

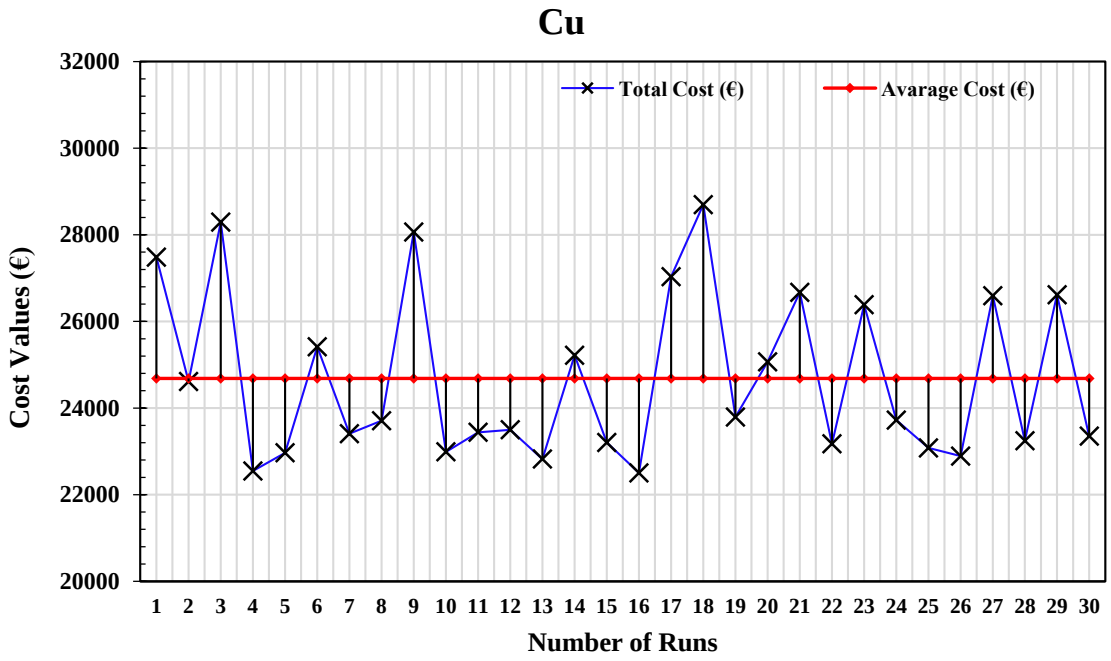

Figure 4.4. Bias (Proximity) graphs of nanofluids based Cu.

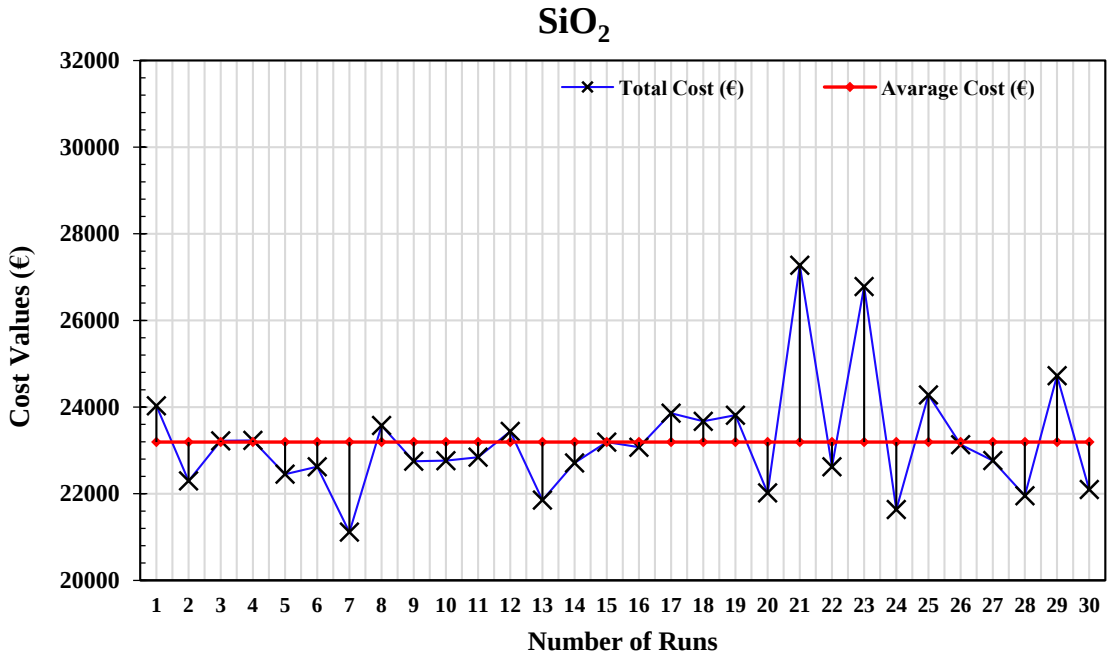

Figure 4.5. Bias (Proximity) graphs of nanofluids based SiO_2.

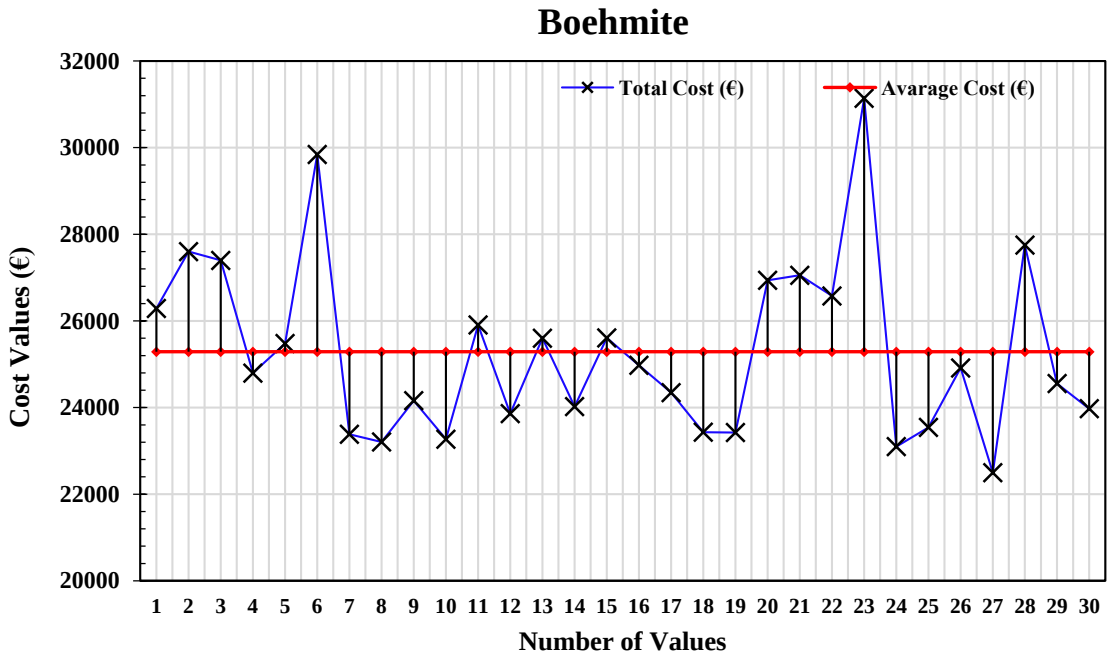

Figure 4.6. Bias (Proximity) graphs of nanofluids based Boehmite.

When the figures are examined, it is seen that the Boehmite values diverge from the average at a very high rate. In addition, CuO and SiO_2 graphs compared to the others, more

stable data are obtained and closer to the average results are obtained. If the CuO and SiO_2 graphs are compared, it is seen that the projection lines moving away from the mean in CuO data are more than the SiO_2 projection lines. The data distribution, in other words in case, the stability is measured by the standard deviation. The standard deviation graph of nanoparticles in AVOA is illustrated in the Figure 4.7.

As predicted when the Bias graphs are examined, it is seen that SiO_2 has the lowest standard deviation data with 1321.44 and Boehmite has the highest standard deviation data with 2060.43. As can be seen in Figure 4.5 and Figure 4.6, the SiO_2 value is the nanofluid with the most stable results among AVOA.

After the stability analysis, the minimum values obtained for each particle and the resulting problem values are examined. The optimum parameters in AVOA of the minimum values of all nanoparticles are shown in Table 4.5.

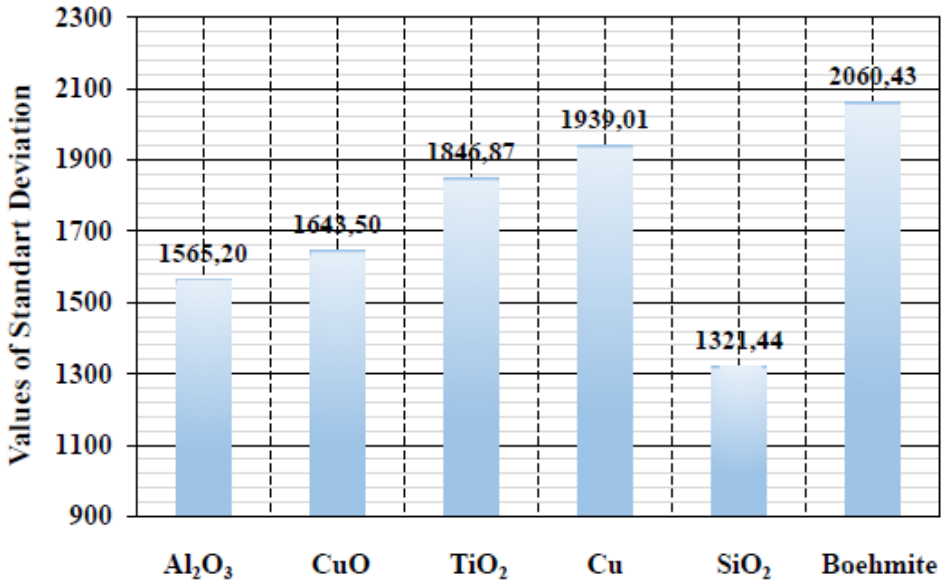

Figure 4.7. The standard deviation of nanoparticles.

If geometric parameters need to be discussed, the same tube layout (45°) and the number of tube passes (2.0) are obtained by each optimizer. It is seen that Boehmite, which has the maximum cost, and Cu, which follows it, also differ compared to the others and the number of passes is 8. In addition, considering the tube length, it is seen that the tube length in the test made with the boehmite particle is longer than the others. (29.8%). When the nanoparticle ratio, which directly affects the problem of parameters such as density,

viscosity, the thermal conductivity of nanofluids, is examined, it is seen that SiO_2, which has the lowest cost, is the solution with including the highest nanoparticle ratio with 4.69 %. In addition, it is seen that the lowest rate is Boehmite with 0.114 %. When the problem variables are examined, it is seen that the first noteworthy data is the number of tubes. The number of tubes is important because it is data that directly concerns the heat conduction surface area between nanofluids and oil. When the number of tubes is compared among each other, the case with Boehmite has only 148 and it is extremely low. On the other hand, the fact that it counts for the longest value among the tube lengths mentioned above, explains why efficiency that is under average is highly low. The fact that the total heat transfer area has the lowest value with 44,981 m^2 proves this argument. It can be also sighted that there is stability among the total number of baffles. When the two data with the lowest efficiency are excluded, it is seen that the other data takes the value of 6. It is seen that the highest value of the overall heat transfer coefficient is SiO_2, which provides the lowest total cost value, as expected. Total discounted cost rates are directly relative with the shell and pipe side pressure drop values.

Table 4.5. Optimal parameters of STHE operated with different nanofluids.

	Al_2O_3	CuO	TiO_2	Cu	SiO_2	Boehmite
Optimization Variables						
Shell-side inside diameter - D_s (m)	0.458	0.449	0.498	0.431	0.427	0.44
Tube-side outside diameter - d_o (mm)	17.6	16.7	20.2	17.1	16.4	22.1
Tube Layout - T_{layout} (°)	45	45	45	45	45	45
Number of tube passes - N_{pass}	2	2	2	2	2	2
Tube length - L (m)	3.1	3.2	3	3.5	3.2	4.4
Tube pitch - p_t (mm)	29.8	29.2	29.8	27.7	28.9	28.7
Central baffle spacing - L_{bc} (m)	0.449	0.483	0.46	0.411	0.464	0.489
Inlet baffle spacing - L_{bi} (m)	0.339	0.469	0.42	0.446	0.468	0.396
Outlet baffle spacing - L_{bo} (m)	0.432	0.494	0.496	0.355	0.454	0.397
Baffle spacing (%)	30.862	33.369	26.974	39.231	31.541	39.552
Width of bypass lane - w_p (mm)	23.6	13.6	19.4	27.5	17.3	15.1
Tube-to-baffle hole diametral clearance - δ_{tb} (mm)	0.6	0.523	0.411	0.417	0.42	0.36
Shell-to-baffle diametral clearance - δ_{sb} (mm)	3.71	3.287	3.354	2.758	4.183	3.598
Number of sealing strip pairs - N_{ss}	2	1	2	8	2	8
Tube thickness - *thck* (mm)	1.1	1.7	1	0.7	1	1.3
The nanoparticle ratio - φ_v (%)	2.887	1.63	3.681	1.967	4.693	0.114
Problem Veriables						
Transverse tube pitch - X_t (mm)	42.2	41.2	42.2	39.2	40.9	40.7
Longitudinal tube pitch - X_l (mm)	21.1	20.6	21.1	19.6	20.5	20.3
Total number of tubes - N	273	292	242	254	271	148
Tube clearance - Cl (mm)	12.2	12.4	9.7	10.6	12.5	6.6
Shell side mass velocity - G_s (kg/m^2 s)	309.373	282.557	347.158	381.912	305.045	505.459
Shell side Reynolds number - Re_s	117.554	101.962	152.412	141.213	107.99	249.403
Shell side heat transfer coefcient - h_s (W/m^{2}K)	519.478	481.563	541.712	511.644	531.697	526.598
Pressure drop in the central section - Δp_{cr} (Pa)	2306.378	1824.566	3178.134	2579.925	2232.91	3533.378
Pressure drop in the window area - Δp_w (Pa)	5453.292	5192.402	5766.242	8039.244	5979.753	10052.98
Pressure drop in inlet and outlet section - $\Delta p_{i\text{-}o}$ (Pa)	4471.186	3163.344	4795.547	5197.129	3748.349	9456.127
Total shell side pressure drop - Δp_{shell} (Pa)	12230.86	10180.31	13739.92	15816.3	11961.01	23042.49
Total number of baffle - N_b	6	6	6	7	6	8
Tube side Reynolds number - Re_t	14175.4	15824.35	13258.55	15259.76	13823.25	22106.07
Tube side heat transfer coefcient - h_i (W/m^2 K)	4037.977	4960.122	3225.385	4008.64	4186.97	4383.557

Table 4.5. Optimal parameters of STHE operated with different nanofluids (More).

	Al_2O_3	**CuO**	**TiO_2**	**Cu**	**SiO_2**	**Boehmite**
Overall heat transfer coefcient - U_o (W/m2 K)	400.535	379.386	404.499	399.302	410.464	408.607
Total heat transfer area - A_o (m^2)	46.456	48.985	46.24	47.022	45.127	44.981
Tube side pressure drop - Δp_t (Pa	3899.914	6897.635	2180.92	4118.028	5522.524	5636.319
Annual operating cost - C_o (€/year)	760.354	712.646	805.026	957.738	783.63	1405.648
Total discounted operating cost - C_{oD} (€)	4672.044	4378.901	4946.535	5884.882	4815.064	8637.1
Capital investment cost - C_i (€)	16524.07	16945.23	16487.95	16618.41	16301.76	16277.39
Total cost of heat exchanger - C_{tot} (€)	21196.11	21324.13	21434.48	22503.29	21116.83	24914.5

As seen in the table, the highest pressure drop in the tube-side is obtained with CuO nanofluid. It is 1375 Pa (19.9%) higher than SiO2, which provides the lowest cost result. The result for CuO is expected, because some obtained geometrical parameters such as number of tube passes and tube length, which are relative with tube side transfer area, seem over the average. Although the lowest pressure drop in the shell part is not directly related to the nanoparticles, it is seen in the Boehmite data with 23042.49 Pa. Comparison of the costs of nanoparticles indicated in the Table 4.5 is visualized in Figure 4.8.

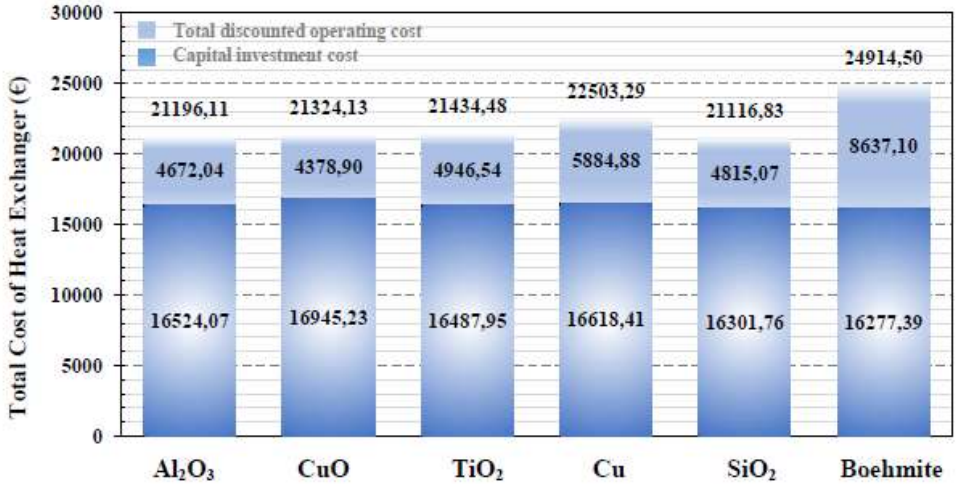

Figure 4.8. Comparison of the total cost values for nanofluids.

Figure 4.8 shows that; capital investment cost of every option is pretty close each other, and V has effective role to determine the optimized value for nanofluids. When Eqn. 28 and Eqn. 29 is considered, capital investment cost is affected by only total heat transfer area while total discounted operating cost is affected by paremeters such as pressure drops, density and efficiency. For this reason, it is usual to see difference among total discounted operating costs. In addition, SiO_2, among other options, provides the optimal solution for a real-world engineering problem with stringent constraints, the shell-and-tube heat exchanger, proving its superiority over other nanoparticles.

Effectiveness of STHE for nanoparticles, which was created based on the data obtained by the algorithm, is given in Figure 4.9.

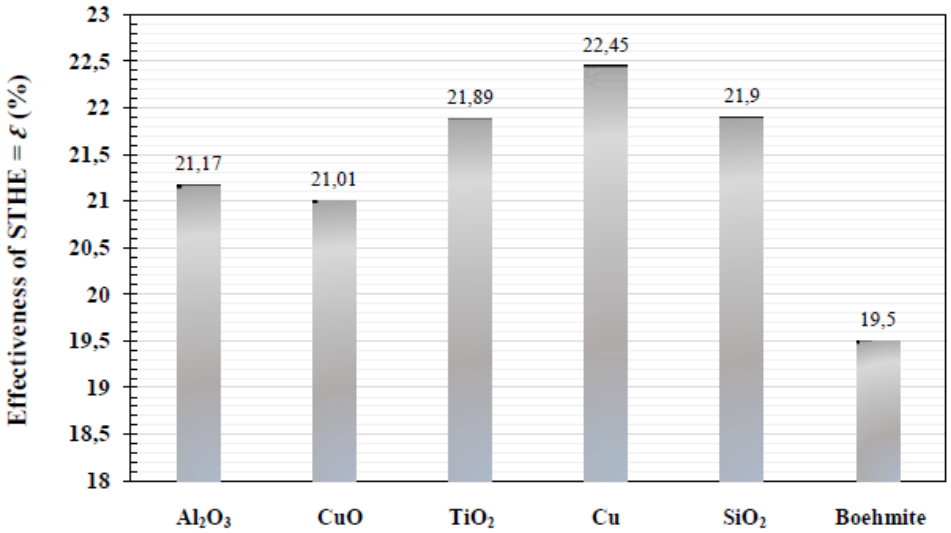

Figure 4.9. Effectiveness of STHE for nanoparticles.

Figure 4.9 indicates the proximity of obtained total heat transfer in STHE to the maximum theoretically achievable total heat transfer; another statement is effectiveness of STHE. According to Figure 4.9, the effectiveness of nanofluid based Cu is the highest while nanofluid based Boehmite is the lowest. In general, the effectiveness of STHE seems low level with 20% - 30%. But it should be considerate that, the optimal result is obtained as a total cost of heat exchanger instead of efficiency. Some geometrical parameters such as total heat transfer area, tube length, tube thickness and number of tube passes, which have significant effects on efficiency, is restricted to obtain best cost for STHE.

As the last stage of the study case, a sensitivity test is performed for the SiO_2 nanoparticle, which is obtained the lowest total cost in the study case. In AVOA, the effect is observed by keeping 15 variables of 16 variables constant and changing the ratios of the remaining 1 data between upper and lower bounders. This process is applied for each variable. The data related to the subject are shown in the Figure 4.10.

When the tube length is taken into account, it is clearly seen that the cost increases (125%) proportionally as the length raises. The reason for this is as follows; Pipe length increases the thermal surface area and, the heat transfer surface area directly affects the capital investment cost in an increasing way although it is necessary for the expected heat transfer. As seen in the number of passes graph, the effect of this variable on the cost is enormous. The difference between the total cost at upper and lower boundaries is about 7700 € (365%) and has the most alteration among the 16 variables. Although the number of

passes has an active effect on the model parameters, its main effect is on the pressure. As can be seen in the formulations mentioned earlier, it directly affects the pressure drop and as the number of passes increases, the pressure raises significantly and thus the cost increases. According to the number of sealing strip pairs graph, it is seen that the N_{ss} variable does not have much effect on the cost. The cost value, which increased by 4, became stable after that. When the Table 3.3 is considered, it can be interpreted that the correction factor for bundle and pass partition bypass streams (J_b) remains constant at 1.0, by exceeding 0.5 for the 4 and 8 values of the N_{ss}^+ value. Difference in tube-to-baffle hole diameter clearance and shell-to-baffle diametric clearance values do not have significant effect on total cost values, on the other hand, it is worth to mention that there is atiny decrease in shell-to-baffle clearance, while the total cost due to tube-to-baffle hole clearance, is approximately steady.

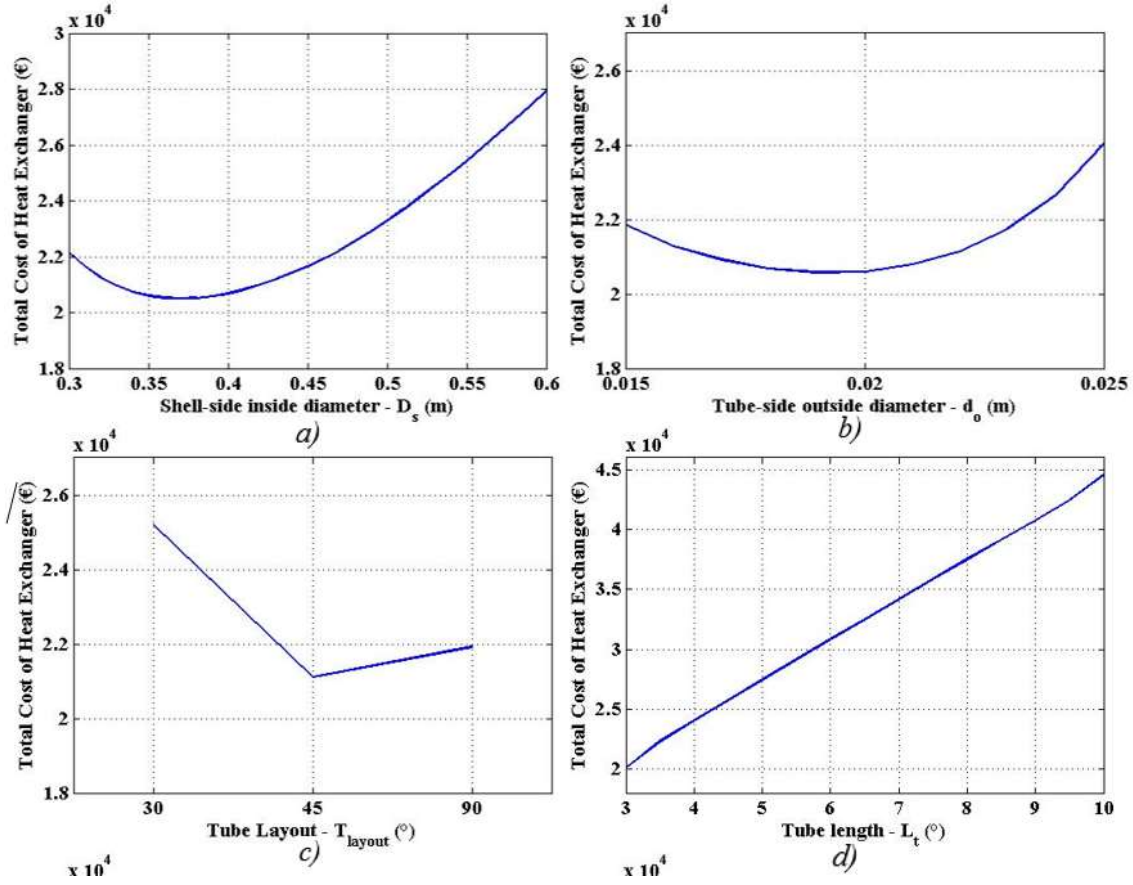

Figure 4.10. Sensitivity analysis of each optimization variables for nanofluid based SiO_2.

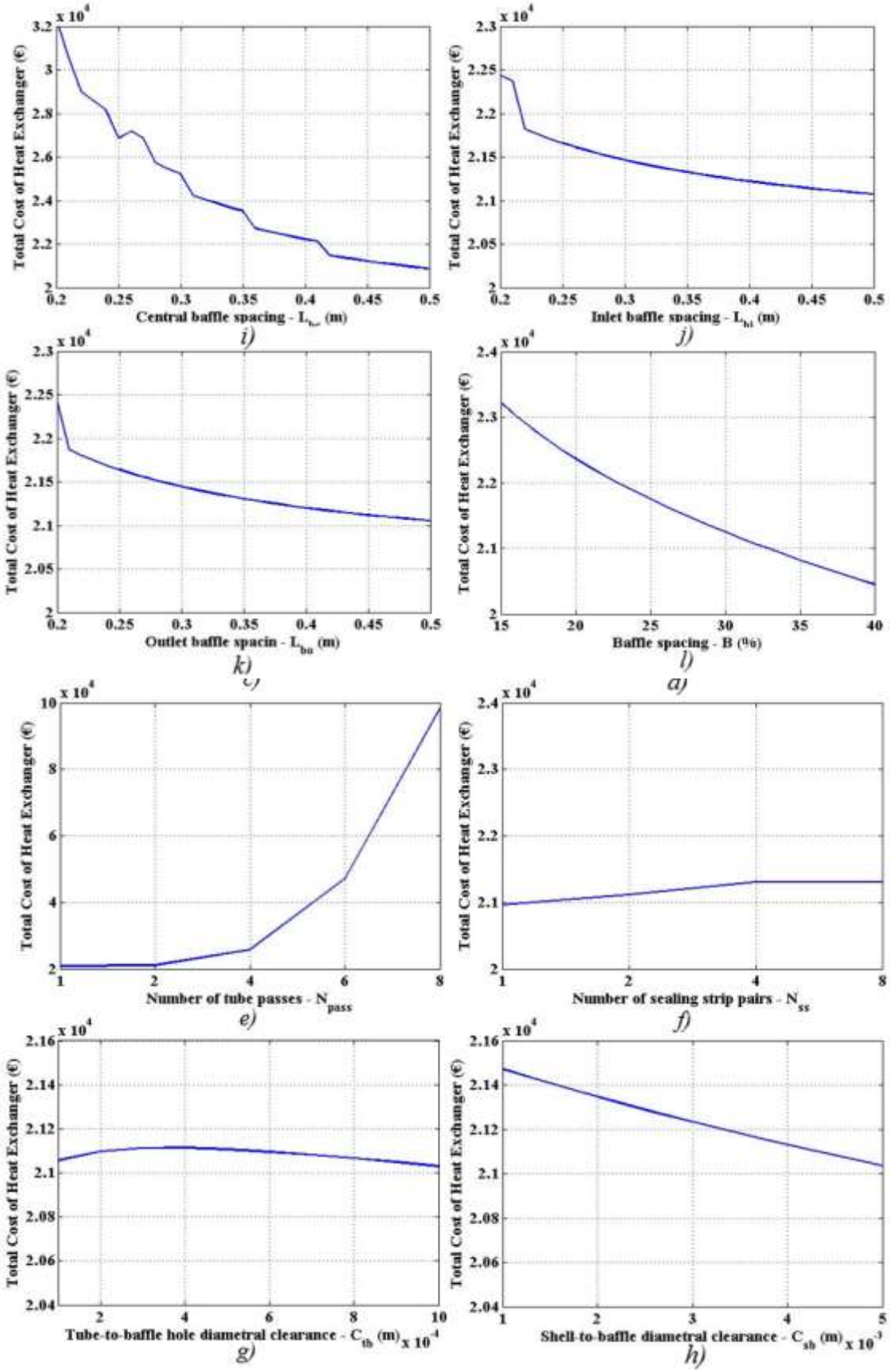

Figure 4.10. Sensitivity analysis of each optimization variables for nanofluid based SiO_2 (More).

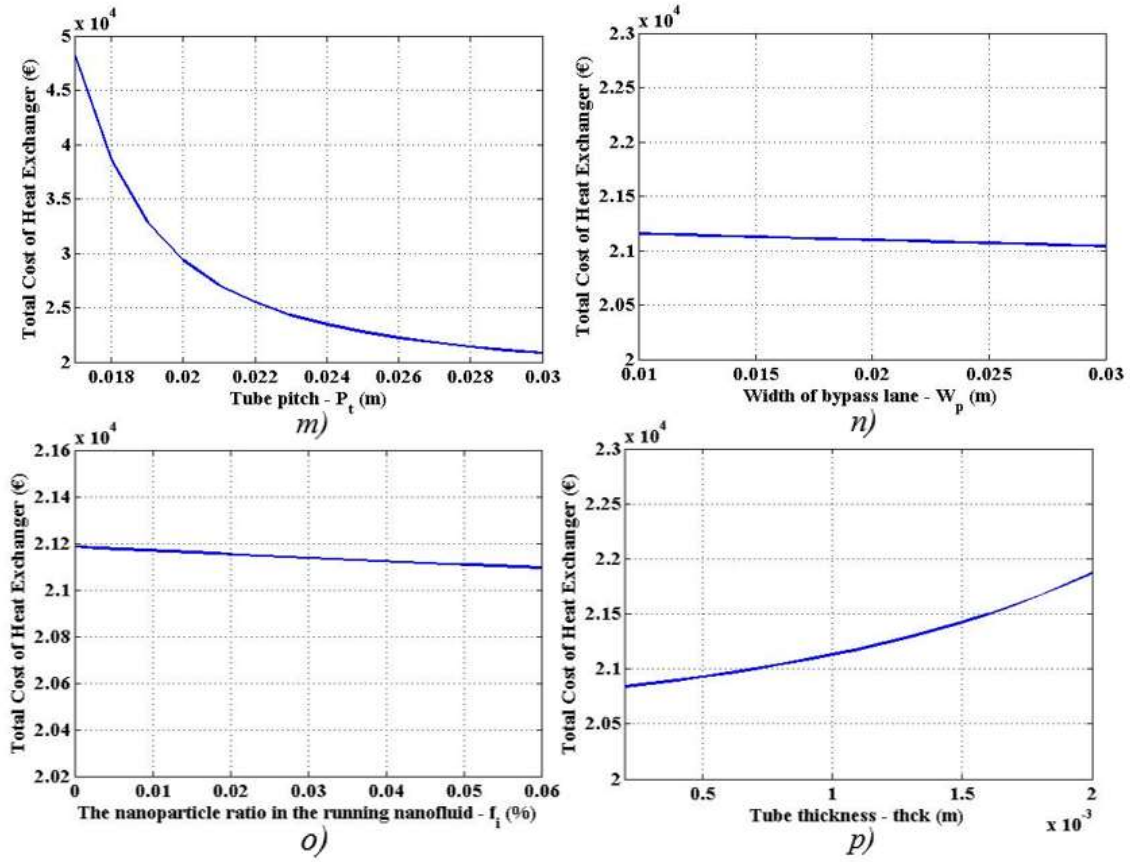

Figure 4.10. Sensitivity analysis of each optimization variables for nanofluid based SiO_2 (More).

When looking at the Baffle spacing graphs, it is observed that the central baffle spacing had a very large effect compared to the inlet baffle spacing and the outlet baffle spacing. As the central baffle spacing increases, the cost is greatly reduced. However, according to all other variables, fluctuations are seen in the variable L_{bc} graph. This is because the central baffle spacing is involved in the formulation of key variables that affect many data, such as fraction of crossflow area available for flow bypass, shell side Reynold number. The similarities of the inlet baffle spacing and the outlet baffle spacing graphs draw attention. It is seen that as these two variables increase, pressure drop in the shell-side inlet and outlet sections decreases, and thus, reducing the cost by declining the shell side pressure drop. Baffle spacing (B) has active role especially in determining the shell side geometrical characteristic. This shows that it is an important variable for shell side pressure drop that directly affects the total cost. When the graph is examined, it is observed that the total cost increases as the percentage of baffle spacing raises. The main reason for this is that, as mentioned above, as baffle spacing raises, the turbulence decreases and the pressure drop

increases in the shell. As seen in the tube pitch graph, the tube pitch has a great influence on the cost. The difference between the upper and lower boundaries is 23700 € (49 % decreasing), which is the second highest rate among the other 15 variables. Just like in baffle spacing, as tube pitch increases, the pressure drop in the shell decreases significantly and the total cost decreases. It is seen that the width of bypass line does not have a great effect on the total cost. However, when graph is examined, it is seen that as the width of bypass line increases, its cost decreases, albeit a little. If nanoparticulate ratio interpreted, it is seen that it does not have a great effect on the cost. However, as the rate increases, there is a slight decrease in the cost. Although the thickness does not have a great effect on the cost, it is observed that the cost increased as the tubes got thicker. The increase in thickness will reduce the inner pipe diameter and reduce the heat transfer and increase the pipe pressure drop, which directly affects the cost, under immediate conditions.

5. CONCLUSION

This work presents a comparison of six different nanofluids for the total cost optimization of a real-world engineering problem STHE with stringent constraints, performed using a meta-heuristic algorithm called African Vulture Optimization Algorithm (AVOA), and determine the most efficient nanofluid. In the thesis, thirty independent simulation results for each six-nanoparticle heat exchanger simulation are obtained by AVOA. Statistical analysis was then performed, Bias (Proximity) and Standard Deviation values were determined for each nanofluid. As a result of statistical analysis, the stability of the data results for AVOA is also measured. After the stability analysis, the restricted real-world problem is solved with AVOA, along with the minimum values obtained for each particle, and the resulting problem values are examined. As the last stage of the study case, a sensitivity test was performed for the SiO_2 nanoparticle, which was obtained the lowest total cost in the study case. In AVOA, the effect was observed by keeping fifteen variables of sixteen variables constant and changing the ratios of the remaining a data between upper and lower bounders. This process was applied for each variable. As a conclusion of this study; although the total cost values are close to each other, Water - SiO_2 nanofluid gave the lowest cost with 21116.83 €. Additionally, the study with SiO_2 nanoparticles gave the most stable results in AVOA, which was used as the meta-heuristic algorithm, and got the lowest standard deviation result of 1321.44. Based on results, it can be said that; while SiO_2 has proven to be the most stable nanoparticle in the algorithm, SiO_2, among other options, provides the optimal solution for a real-world engineering problem with stringent constraints, the shell-and-tube heat exchanger, proving its superiority over other nanoparticles.

REFERENCES

Abbasian Arani, A. A. and Moradi, R. (2019) 'Shell and tube heat exchanger optimization using new baffle and tube configuration', *Applied Thermal Engineering*, 157(April). doi: 10.1016/j.applthermaleng.2019.113736.

Abdollahzadeh, B. *et al.* (2021) 'African vultures optimization algorithm: A new nature-inspired metaheuristic algorithm for global optimization problems', *Computers and Industrial Engineering* 158(1), doi: 10.1016/j.cie.2021.107408

Alazwari, M. A. and Safaei, M. R. (2021) 'Combination effect of baffle arrangement and hybrid nanofluid on thermal performance of a shell and tube heat exchanger using 3-d homogeneous mixture model', *Mathematics*, 9(8). doi: 10.3390/math9080881.

Anitha, S. *et al.* (2019) 'What dominates heat transfer performance of hybrid nanofluid in single pass shell and tube heat exchanger?', *Advanced Powder Technology*, 30(12), pp. 3107–3117. doi: 10.1016/j.apt.2019.09.018.

Arad, Z. and Bernstein, M. H. (1988) 'Temperature Regulation in Turkey Vultures', *The Condor*, 90(4), pp. 913–919. doi: 10.2307/1368848.

Asadi, M. *et al.* (2014) 'Economic optimization design of shell-and-tube heat exchangers by a cuckoo-search-algorithm', *Applied Thermal Engineering*, 73(1), pp. 1032–1040. doi: 10.1016/j.applthermaleng.2014.08.061.

Blum, C. and Roli, A. (2003) 'Metaheuristics in Combinatorial Optimization: Overview and Conceptual Comparison', *ACM Computing Surveys*, 35(3), pp. 268–308. doi: 10.1145/937503.937505.

Bosè, M. and Sarrazin, F. (2007) 'Competitive behaviour and feeding rate in a reintroduced population of Griffon Vultures Gyps fulvus', *Ibis*, 149(3), pp. 490–501. doi: 10.1111/j.1474-919X.2007.00674.x.

Clary, D. R. and Mills, G. (2011) 'Preparation and thermal properties of CuO particles', *Journal of Physical Chemistry C*, 115(5), pp. 1767–1775. doi: 10.1021/jp110102r.

Dubey, V. V. P. *et al.* (2014) 'Performance Analysis of Shell & Tube Type Heat Exchanger under the Effect of Varied Operating Conditions', 11(3), pp. 8–17.

ETSU (2000) ‘Compact Heat Exchangers - Guidance for Engineers’, p. 255.

Fan, Y., Luo, L. and Flamant, G. (2013) ‘Design of Compact Heat Exchangers for Transfer Intensification’, in *Heat and Mass Transfer Intensification and Shape Optimization*. London: Springer London, pp. 81–111. doi: 10.1007/978-1-4471-4742-8_4.

Farajollahi, B., Etemad, S. G. and Hojjat, M. (2010) ‘Heat transfer of nanofluids in a shell and tube heat exchanger’, *International Journal of Heat and Mass Transfer*, 53(1–3), pp. 12–17. doi: 10.1016/j.ijheatmasstransfer.2009.10.019.

Fesanghary, M., Damangir, E. and Soleimani, I. (2009) ‘Design optimization of shell and tube heat exchangers using global sensitivity analysis and harmony search algorithm’, *Applied Thermal Engineering*. doi: 10.1016/j.applthermaleng.2008.05.018.

Fettaka, S., Thibault, J. and Gupta, Y. (2013) ‘Design of shell-and-tube heat exchangers using multiobjective optimization’, *International Journal of Heat and Mass Transfer*, 60(1), pp. 343–354. doi: 10.1016/j.ijheatmasstransfer.2012.12.047.

Gharehchopogh, F. S. and Gholizadeh, H. (2019) ‘A comprehensive survey: Whale Optimization Algorithm and its applications’, *Swarm and Evolutionary Computation*, 48(March), pp. 1–24. doi: 10.1016/j.swevo.2019.03.004.

Ghozatloo, A., Rashidi, A. and Shariaty-Niassar, M. (2014) ‘Convective heat transfer enhancement of graphene nanofluids in shell and tube heat exchanger’, *Experimental Thermal and Fluid Science*, 53, pp. 136–141. doi: 10.1016/j.expthermflusci.2013.11.018.

Gopal, A., Sultani, M. M. and Bansal, J. C. (2020) ‘On Stability Analysis of Particle Swarm Optimization Algorithm’, *Arabian Journal for Science and Engineering*, 45(4), pp. 2385–2394. doi: 10.1007/s13369-019-03991-8.

Heat Exchanger, Space heating equipment (2015) *Navjoyt Engineering Works And Equipments Pvt. Ltd.* Available at: http://navjyot.co.in/heat-exchanger.html (Accessed: 20 January 2021).

Houston, D. C. (1974) ‘The role of griffon vultures Gyps africanus and Gyps ruppellii as scavengers’, *Journal of Zoology*, 172(1), pp. 35–46. doi: 10.1111/j.1469-7998.1974.tb04092.x.

Jia, H. *et al.* (2019) ‘Dynamic Harris hawks optimization with mutation mechanism for satellite image segmentation’, *Remote Sensing*, 11(12). doi: 10.3390/rs11121421.

Kakaç, S. and Liu, H. (2002) *Heat exchangers: Selection, rating, and thermal design, second edition, Heat Exchangers: Selection, Rating, and Thermal Design, Second Edition*.

Kayabasi, E., Alperen, M. A. and Kurt, H. (2019) ‘The effects of component dimensions on heat transfer and pressure loss in shell and tube heat exchangers’, *International Journal of Green Energy*, 16(2), pp. 200–210. doi: 10.1080/15435075.2018.1555162.

Kendall, C. *et al.* (2012) ‘Mechanisms of coexistence in vultures: Understanding the patterns of vulture abundance at carcasses in Masai Mara National Reserve, Kenya’, *Condor*, 114(3), pp. 523–531. doi: 10.1525/cond.2012.100196.

Lamella Heat Exchangers (1999) *Sondex Tapiro Oy Ab*. Available at: http://tapiro.fi/tuotteet/lammonsiirtimet_e.html (Accessed: 15 July 2020).

Lotfi, R., Rashidi, A. M. and Amrollahi, A. (2012) ‘Experimental study on the heat transfer enhancement of MWNT-water nanofluid in a shell and tube heat exchanger’, *International Communications in Heat and Mass Transfer*, 39(1), pp. 108–111. doi: 10.1016/j.icheatmasstransfer.2011.10.002.

Mohanty, D. K. (2016) ‘Application of firefly algorithm for design optimization of a shell and tube heat exchanger from economic point of view’, *International Journal of Thermal Sciences*, 102, pp. 228–238. doi: 10.1016/j.ijthermalsci.2015.12.002.

Parıldar, H. (2020) ‘Infectious Disease Outbreaks in History’, *The journal of Tepecik Education and Research Hospital*, 30, pp. 19–26. doi: 10.5222/terh.2020.93764.

Patel, V. *et al.* (2021) ‘Qualitative and Quantitative Performance Comparison of Recent Optimization Algorithms for Economic Optimization of the Heat Exchangers’, *Archives of Computational Methods in Engineering*, 28(4), pp. 2881–2896. doi: 10.1007/s11831-020-09479-1.

Ram, M. *et al.* (2022) ‘Job creation during a climate compliant global energy transition across the power, heat, transport, and desalination sectors by 2050’, *Energy*, 238, p. 121690. doi: 10.1016/j.energy.2021.121690.

Rotary Type Regenerator (2016) *ÖSTBERG GROUP AB*. Available at: https://na.ostberg.com/wp-content/uploads/sites/25/2016/02/heatexchanger.png (Accessed: 15 July 2020).

Ruxton, G. D. and Houston, D. C. (2004) 'Obligate vertebrate scavengers must be large soaring fliers', *Journal of Theoretical Biology*, 228(3), pp. 431–436. doi: 10.1016/j.jtbi.2004.02.005.

Sadeghzadeh, H., Aliehyaei, M. and Rosen, M. A. (2015) 'Optimization of a finned shell and tube heat exchanger using a multi-objective optimization genetic algorithm', *Sustainability (Switzerland)*, 7(9), pp. 11679–11695. doi: 10.3390/su70911679.

Shah, R. K. and Sekuli, D. P. (2003) *Fundamentals of Heat Exchanger Design*, *Fundamentals of Heat Exchanger Design*. doi: 10.1002/9780470172605.

Shell & tube heat exchanger - EnggCyclopedia (2011). Available at: https://www.enggcyclopedia.com/2019/04/shell-tube-heat-exchanger/ (Accessed: 30 March 2022).

Smith, E. M. (2005) *Advances in Thermal Design of Heat Exchangers - A numerical approach: direct-sizing, step-wise rating and transients*.

Sonawane, S. S., Khedkar, R. S. and Wasewar, K. L. (2015) 'Effect of sonication time on enhancement of effective thermal conductivity of nano TiO2–water, ethylene glycol, and paraffin oil nanofluids and models comparisons', *Journal of Experimental Nanoscience*, 10(4), pp. 310–322. doi: 10.1080/17458080.2013.832421.

Spiral Heat Exchanger Internal (2018) *Piping Engineering*. Available at: https://www.pipingengineer.org/spiral-heat-exchangers-equipment-and-piping-layout/spiral-heat-exchanger/ (Accessed: 20 January 2021).

Taal, M. *et al.* (2003) 'Cost estimation and energy price forecasts for economic evaluation of retrofit projects', *Applied Thermal Engineering*, 23(14), pp. 1819–1835. doi: 10.1016/S1359-4311(03)00136-4.

The Flat Plate Heat Exchanger in Comparison with Other Types of Heat Exchangers (2010) *Bright Hub Engineering*. Available at: https://www.brighthubengineering.com/hvac/61791-features-and-characteristics-of-the-flat-plate-heat-exchanger/ (Accessed: 20 January 2021).

Tubular Heat Exchangers Manufacturers Association (1999) ‘Standards of the Tubular Exchangers Manufacturers Association’, *Main*, p. 294.

Turgut, M. S. and Turgut, O. E. (2020) *Global best-guided oppositional algorithm for solving multidimensional optimization problems*, *Engineering with Computers*. Springer London. doi: 10.1007/s00366-018-0684-5.

Turgut, O. E., Turgut, M. S. and Coban, M. T. (2014) ‘Design and economic investigation of shell and tube heat exchangers using Improved Intelligent Tuned Harmony Search algorithm’, *Ain Shams Engineering Journal*. doi: 10.1016/j.asej.2014.05.007.

Vahdat Azad, A. and Vahdat Azad, N. (2016) ‘Application of nanofluids for the optimal design of shell and tube heat exchangers using genetic algorithm’, *Case Studies in Thermal Engineering*, 8, pp. 198–206. doi: 10.1016/j.csite.2016.07.004.

Vulture Facts (2011). Available at: https://web.archive.org/web/20110718015236/http://www.webvulture.com/vulture-facts.html (Accessed: 17 October 2021).

Vultures Circling Overhead - The Emergence Network (2019). Available at: http://www.emergencenetwork.org/project-index/vultures-circling-overhead/ (Accessed: 4 January 2022).

Xue, Y. *et al.* (2018) ‘An Evolutionary Computation Based Feature Selection Method for Intrusion Detection’, *Security and Communication Networks*, 2018. doi: 10.1155/2018/2492956.

Żyła, G. and Fal, J. (2017) ‘Viscosity, thermal and electrical conductivity of silicon dioxide–ethylene glycol transparent nanofluids: An experimental studies’, *Thermochimica Acta*, 650, pp. 106–113. doi: 10.1016/j.tca.2017.02.001.

T.C.

AYDIN ADNAN MENDERES UNIVERSITY

GRADUATE SCHOOL OF NATURAL AND APPLIED SCIENCES

SCIENTIFIC ETHICAL STATEMENT

I hereby declare that I composed all the information in my master's thesis entitled "THERMAL DESIGN AND OPTIMIZATION OF SHELL AND TUBE HEAT EXCHANGER THROUGH METAHEURISTIC ALGORITHMS" within the framework of ethical behavior and academic rules, and that due references were provided and for all kinds of statements and information that do not belong to me in this study in accordance with the guide for writing the thesis. I declare that I accept all kinds of legal consequences when the opposite of what I have stated is revealed.

Hayrullah Bilgeran YEŞİLÖZ

27 /06 / 2022

CURRICULUM VITAE

Last name, First Name : YEŞİLÖZ, Hayrullah Bilgeran

Nationality **:** Turkish

Place of birth and date :

Telephone **:**

Email **:**

Foreign language **:** English (IELTS = 6.0)

EDUCATION

Level	Institute	Date of graduation
Master's	Aydın Adnan Menderes University – Mechanical Engineering	August 2022
Bachelor's	Gazi University – Energy Systems Engineering	June 2018

WORK EXPERIENCE

Year	Place / Institute	Title
2017 – 2018	ASELSAN A.Ş.	Engineer Candidate
2022 - Currently	SIMER SAC A.Ş.	Project Engineer